

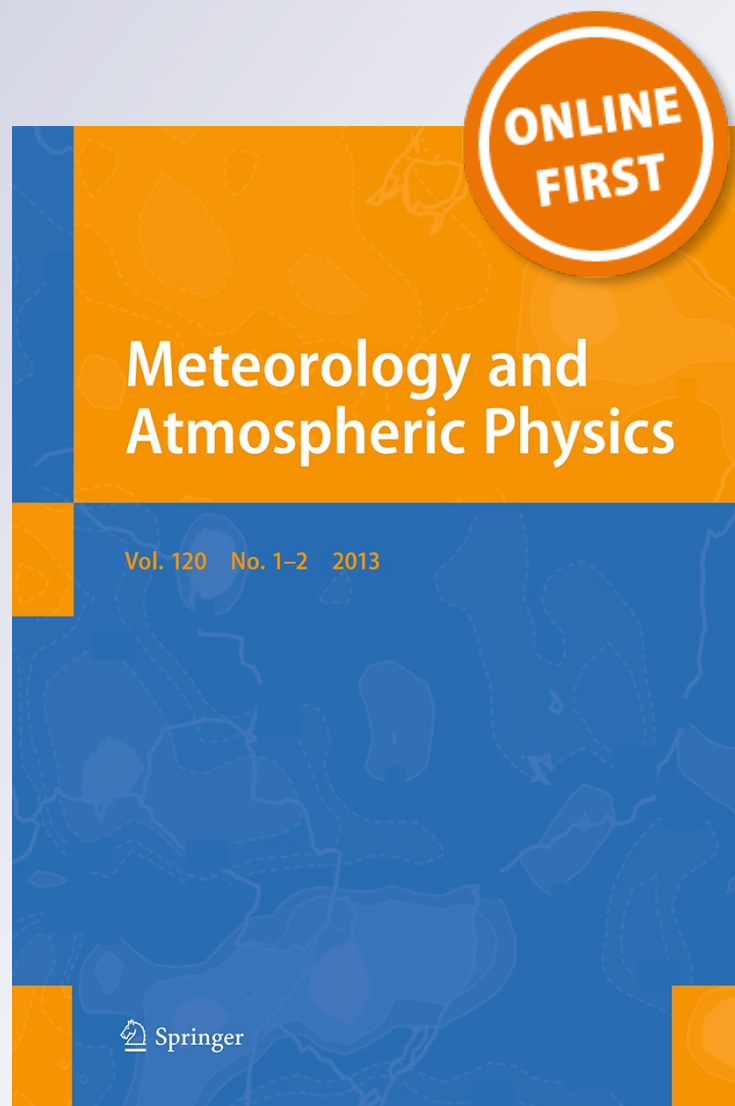
*Origin of the pre-tropical storm Debby
(2006) African easterly wave-mesoscale
convective system*

**Yuh-Lang Lin, Liping Liu, Guoqing
Tang, James Spinks & Wilson Jones**

**Meteorology and Atmospheric
Physics**

ISSN 0177-7971

Meteorol Atmos Phys
DOI 10.1007/s00703-013-0248-6



Your article is protected by copyright and all rights are held exclusively by Springer-Verlag Wien. This e-offprint is for personal use only and shall not be self-archived in electronic repositories. If you wish to self-archive your work, please use the accepted author's version for posting to your own website or your institution's repository. You may further deposit the accepted author's version on a funder's repository at a funder's request, provided it is not made publicly available until 12 months after publication.

Origin of the pre-tropical storm Debby (2006) African easterly wave-mesoscale convective system

Yuh-Lang Lin · Liping Liu · Guoqing Tang ·
James Spinks · Wilson Jones

Received: 16 September 2011 / Accepted: 7 March 2013
© Springer-Verlag Wien 2013

Abstract The origins of the pre-Debby (2006) mesoscale convective system (MCS) and African easterly wave (AEW) and their precursors were traced back to the southwest Arabian Peninsula, Asir Mountains (AS), and Ethiopian Highlands (EH) in the vicinity of the ITCZ using satellite imagery, GFS analysis data and ARW model. The sources of the convective cloud clusters and vorticity perturbations were attributed to the cyclonic convergence of northeasterly Shamal wind and the Somali jet, especially when the Mediterranean High shifted toward east and the Indian Ocean high strengthened and its associated Somali jet penetrated farther to the north. The cyclonic vorticity perturbations were strengthened by the vorticity stretching associated with convective cloud clusters in the genesis

region—southwest Arabian Peninsula. A conceptual model was proposed to explain the genesis of convective cloud clusters and cyclonic vorticity perturbations preceding the pre-Debby (2006) AEW–MCS system.

1 Introduction

It is well documented that most tropical cyclones (TCs) in the main development region (MDR, including tropical North Atlantic and Caribbean Sea, primarily between 10° and 20°N) of Atlantic hurricanes formed from African Easterly Waves (AEWs) (e.g., Carlson 1969; Frank 1970; Goldenberg and Shapiro 1996). Some of the AEWs that did not spawn hurricanes in MDR continued to propagate westward across the Atlantic and then spawned hurricanes in eastern Pacific on the lee of Central American Mountains (e.g., Bister and Emanuel 1997; Farfan and Zehnder 1997). AEW-induced tropical cyclones account for about 60 % of the Atlantic basin tropical storms and non-major hurricanes, but about 85 % of the major hurricanes (categories 3, 4 and 5) (Landsea 1993). Note that the major hurricanes account for just over 20 % of the tropical storms and hurricanes that strike the United States, but cause more than 80 % of the damage (Pielke and Landsea 1998). Thus, understanding the origins and formation mechanisms of the AEWs is essential in improving the forecast of Atlantic hurricanes.

Based on the definition in the Glossary of Meteorology (Glickman 2000), an easterly wave is a migratory wavelike disturbance of the tropical easterlies. It is a wave within the broad easterly current and moves from east to west, generally more slowly than the current in which it is embedded. Thus, African easterly waves may be defined as easterly waves observed over North Africa. In addition,

Responsible editor: F. Mesinger.

Y.-L. Lin
Department of Physics, North Carolina A&T State University,
Greensboro, NC 27411, USA

Y.-L. Lin · J. Spinks
Department of Energy and Environmental Systems,
North Carolina A&T State University,
Greensboro, NC 27411, USA

Y.-L. Lin
NOAA ISET Center, North Carolina A&T State University,
Greensboro, NC 27411, USA

Y.-L. Lin (✉)
EES/ISET, North Carolina A&T State University,
1601 E. Market St., 302H Gibbs Hall, Greensboro,
NC 27411, USA
e-mail: ylin@ncat.edu

L. Liu · G. Tang · W. Jones
Department of Mathematics, North Carolina A&T State
University, Greensboro, NC 27411, USA

observational analyses indicated that AEWs possess the following basic characteristics (e.g., Chen 2006): (1) propagation speeds of $7\text{--}9\text{ ms}^{-1}$, (2) wavelengths of $\sim 2,000\text{--}4,000\text{ km}$, (3) propagating along the rainy zone and to the south of the African easterly jet (AEJ) around 10°N (AEW_s) or along the Saharan thermal low near 20°N (AEW_n) (e.g., Reed et al. 1977; Burpee 1974; Chen 2006), and (4) the maximum intensity of AEWs is near the 700 hPa level. Note that it was also proposed that the vorticity centers of AEW_n and AEW_s propagate together as part of a single AEW (see e.g., Carlson 1969, Burpee 1974, Reed et al. 1977, Pytharoulis and Thorncroft 1999). Similar to the pre-Alberto (2000) AEW (Lin et al. 2005), the pre-Debby (2006) AEW propagated along 10°N and thus can be identified as a AEW_s . Several mechanisms have been proposed in the past to explain the formation of AEWs (see Chen 2006 for a brief review). First, the Charney and Stern (1962) barotropic–baroclinic instability was proposed by Burpee (1972), which is more applicable for $\text{AEW}_{s,s}$ (e.g., Rennick 1976; Mass 1979; Kwon 1989; Thorncroft and Hoskins 1994a, b). Secondly, the baroclinic instability was proposed by Chang (1993) and Thorncroft (1995), which seems to be more applicable for $\text{AEW}_{n,s}$. This mechanism may include the so-called AEJ instability (e.g., Simmons 1977; Thorncroft and Hoskins 1994a, b; Grist et al. 2002) since the AEJ is supported by the baroclinicity associated with the Sahara desert. Thirdly, the convective heating associated with the intertropical convergence zone (ITCZ) has also been proposed to explain the formation of AEWs (e.g., Hsieh and Cook 2005, 2007; Thorncroft et al. 2008). Latent heating may also act together with barotropic/baroclinic instability. Fourthly, the orographic forcing has also been proposed as a formation mechanism of AEWs (Carlson 1969; Mozer and Zehnder 1996; Hill and Lin 2003; Lin et al. 2005; Berry and Thorncroft 2005). In addition, AEWs can also be strengthened by cyclonic vorticity (mesoscale convective vortices—MCVs) produced by MCSs.

These existing mechanisms may help us identify the potential origins of the AEW. However, searching for the origins of AEWs, such as the pre-Debby AEW, will add new understanding or mechanisms to the list. For example, in searching for the origin of pre-Alberto (2000) AEW and MCS, it was found that orographic forcing associated with EH may serve as a formation mechanism of AEW.

Although a number of previous studies indicated that AEW could not be detected in Eastern Africa (e.g. Burpee 1972), Hill and Lin (2003) and Lin et al. (2005) have traced the pre-Alberto (2000) MCS system and its precursor to the EH and proposed that the AEW–MCS system was initiated by the EH. The analysis of Meteosat satellite imagery indicated about 68 % of the eastern Atlantic tropical cyclones originated from the EH region during the period

of 1990–2001 (Lin et al. 2005). On the other hand, Berry and Thorncroft (2005) proposed that the pre-Alberto AEW was initiated by convection over the Darfur Mountains. Note that the MCS is not necessarily associated with AEW during their early formation stage in eastern Africa.

AEWs often have MCSs embedded within them while traveling westward (e.g., Payne and McGarry 1977; Laing and Fritsch 1993; Fink and Reiner 2003). These MCSs help modulate rainfall over the African continent on a daily basis (e.g., Carlson 1969) and help make AEWs detectable from the satellite imagery. Based on the analysis of satellite imagery and ECMWF reanalysis data, Mekonnen et al. (2006) found that the Darfur Mountains are particularly important for providing convective precursors that propagate westward and trigger AEWs downstream. On the other hand, as mentioned above, Lin et al. (2005) found that the diurnally induced MCS over the EH was able to combine with the AEW, which was produced nearby, to form the pre-Alberto AEW–MCS system. In West Africa, some MCSs, such as squall lines and cloud clusters, are found to be modulated by AEWs (Laing et al. 2008).

In this study, we make distinction between the pre-Debby MCS/cloud clusters and AEW, and examine closely the evolution of the pre-Debby (2006) AEW and MCSs in EH, Darfur Mountains (DF), Asir Mountains (AS), and southern Arabian Peninsula to gain more understanding of the origins of the pre-TC AEWs. We also investigate the sources of both the convective cloud clusters and vorticity perturbations and how they were strengthened.

The paper is organized as follows. Section 2 discusses the origin and propagation of the pre-Debby (2006) MCS/cloud clusters, based on the satellite imagery. Section 3 applies the Advanced Research WRF (ARW) model to investigate the origins and propagation of the pre-Debby MCS and AEW. Origins of both the convective cloud clusters and vorticity perturbations prior to the pre-Debby MCS and AEW, respectively, will also be discussed in Sect. 3. Concluding remarks can be found in Sect. 4. Lastly, the description of the ARW model and the numerical experiments designed for this study are given in the “Appendix”.

2 Origin of the Pre-Debby (2006) MCS/cloud clusters and AEW

The Meteosat 8 infrared (IR) images with 6 h interval are used to trace the pre-Debby (2006) MCS or cloud clusters (AMMA 2006). The pre-Debby MCS can be traced back to 1800 UTC 16 August (8/16/18Z) 2006 approximately located at (20°E , 12°N) on the lee side of the southwest Darfur Mountains near southeast Chad (denoted as “D” in Fig. 1b) from its tropical storm stage over the eastern North Atlantic Ocean at 8/22/18Z (Fig. 1d).

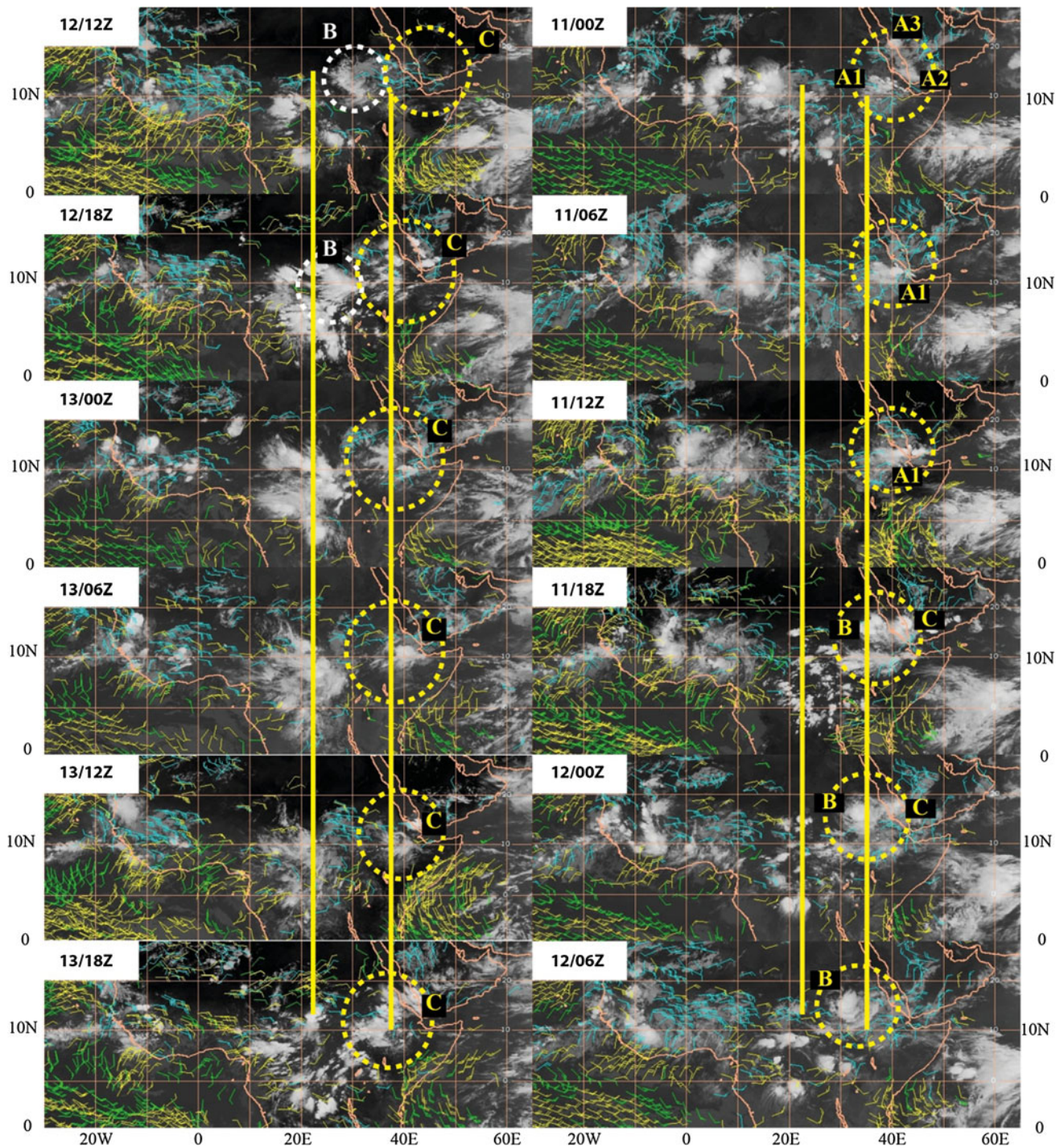


Fig. 1 Meteosat-8 infrared (IR) clouds and wind vectors for every 6 h starting from 8/11/00Z to 8/22/18Z 2006 (AMMA 2006). The center latitude is 10°N. Track of the approximate locations of the pre-Debby (2006) MCS or convective cloud clusters are highlighted by dotted yellow and white circles. The dotted white circles denote the cloud clusters which were not related to the pre-Debby MCS identified at

8/16/18Z. The right (left) yellow line denotes the diurnal convection mode (diurnal cycle) of orographic cloud clusters over the Ethiopian Highlands (Darfur Mountains). The wind vectors were analyzed by Meteosat-8 and are denoted as: blue for 400–599 mb, yellow for 600–799 mb, and green for 800–950 mb)

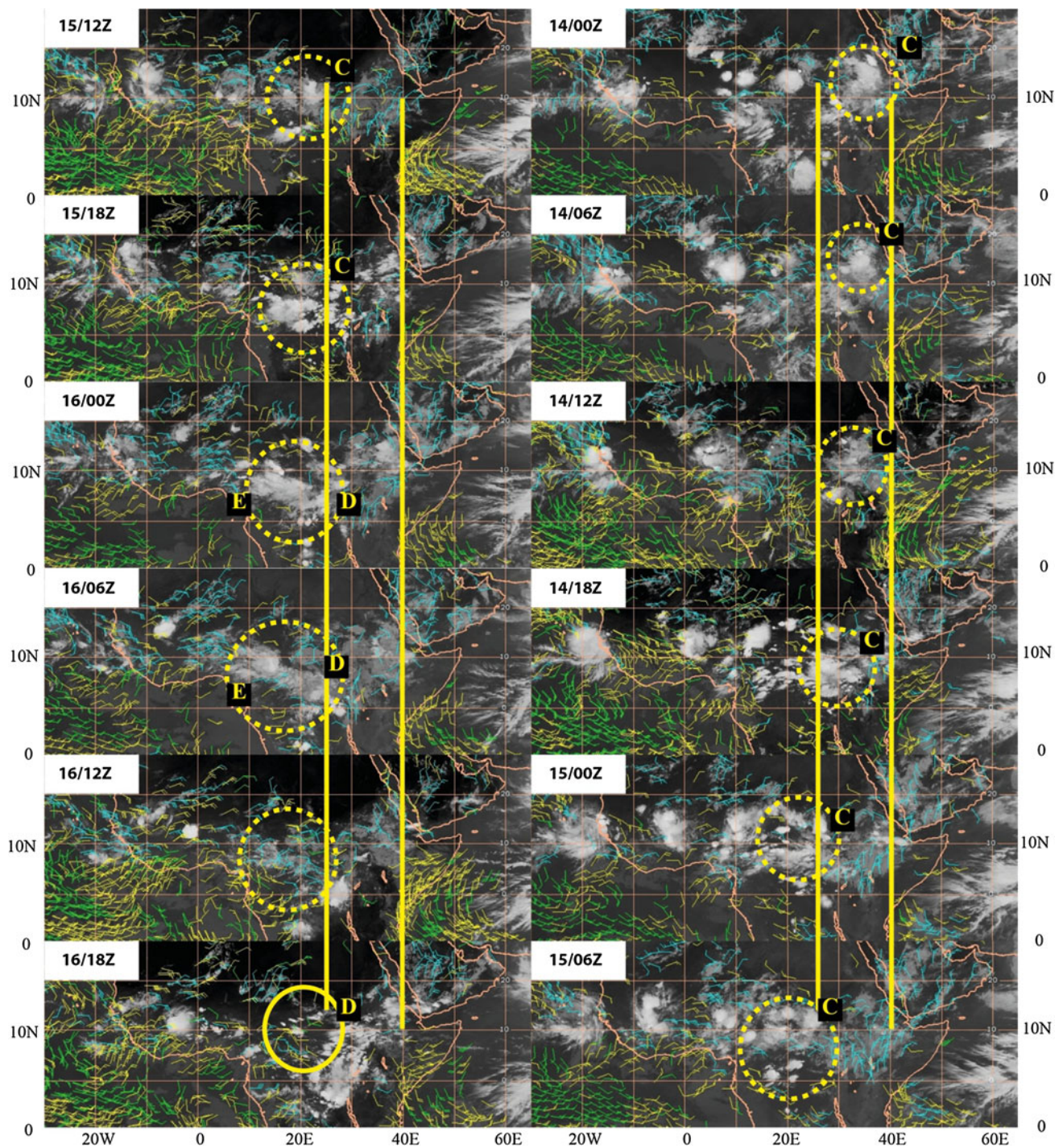


Fig. 1 continued

2.1 Merging of cloud clusters into the Pre-Debby MCS before 1800 UTC August 16

Before 8/16/18Z, the pre-Debby MCS can be further traced back to EH and AS as a series of cloud clusters (A1–A3, B, C, D and E in Fig. 1a, b). For convenience, the general

geography of Africa and Arabian Peninsula is provided in Fig. 2a. During the period 8/8/06Z to 8/10/00Z (not shown), a series of cloud clusters developed at (35°–40°E, 10°–15°N) over the EH and AS (see Tables 1, 2 for acronyms and Fig. 2 for geography). These convective cloud clusters (CCCs) went through growing, splitting, advection, weakening, and

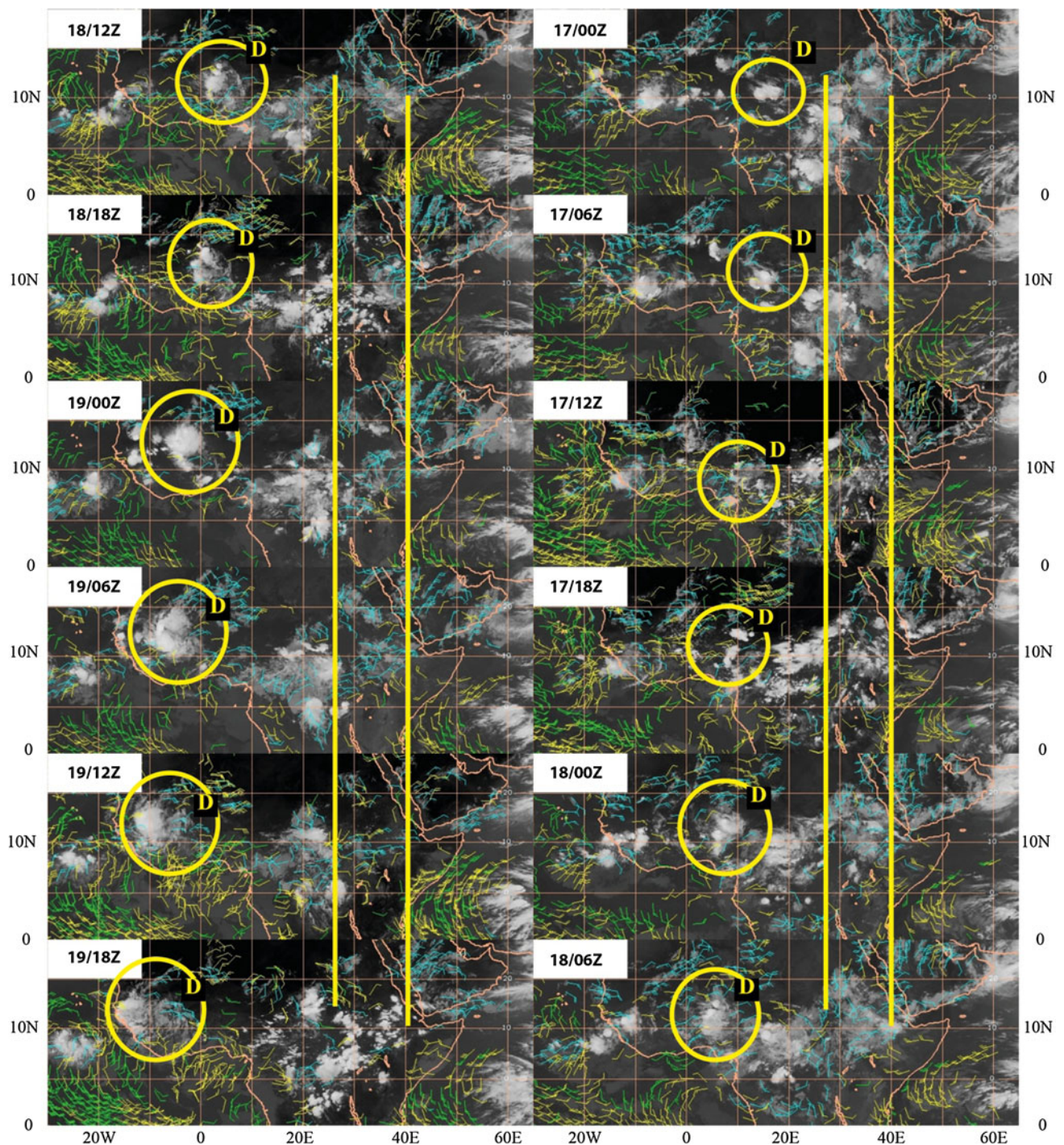


Fig. 1 continued

merging processes, then propagated westward across the North African continent at later times. During these processes, not every individual CCC survived and propagated at the same speed. Another series of CCCs developed on 10–11 August over southwest Arabian Peninsula, AS, and EH at (35°–45°E, 10°–15°N). In fact, three CCCs over this area at 8/11/00Z can be identified (A1–A3 in Fig. 1a). In the next

24 h, the cloud cluster A1 over EH grew stronger, while the other two cloud clusters A2 and A3 over Red Sea and AS dissipated. Cloud cluster A1 over EH then split into two cloud clusters (B and C) around 8/11/18Z. Cloud cluster B started to propagate away from the EH, went through growing and splitting processes while it propagated further downstream prior to the pre-Debby MCS.

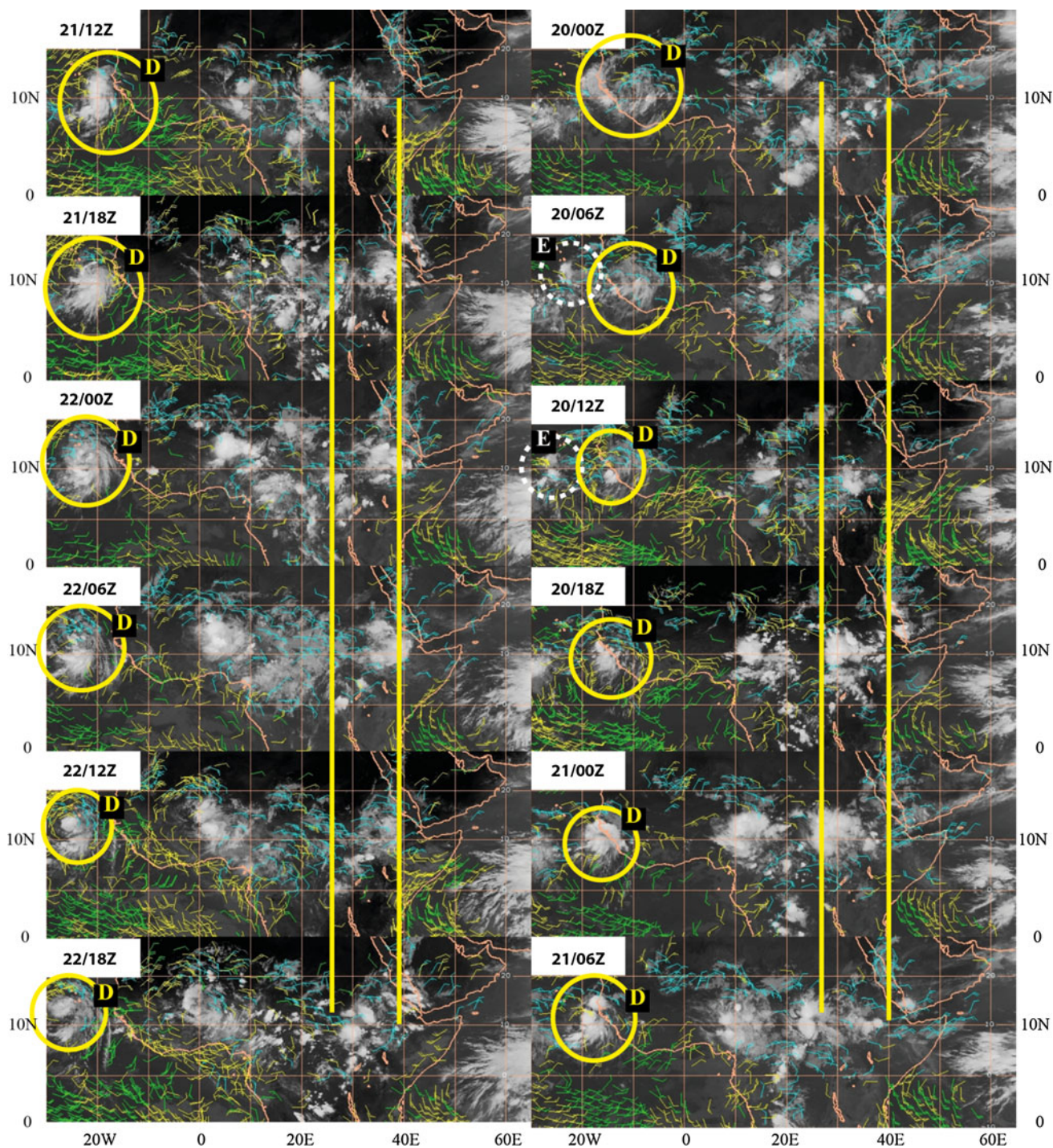


Fig. 1 continued

Cloud cluster C (Fig. 1a) at 8/12/00Z over the Red Sea dissipated in the next 12 h as it went through the nocturnal cycle of the orographic convection over EH and Red Sea. At 8/12/18Z, cloud cluster C redeveloped over EH and AS mountains. The convective clouds contained in this cloud cluster merged into a single, small, but much stronger cloud cluster around 8/13/06Z. Similar splitting and weakening

processes repeated during the period 8/13/06Z to 8/14/00Z (Fig. 1a, b). The merged cloud cluster C (Fig. 1b) propagated to the northwest of EH by 8/14/00Z, mainly being advected by the northeasterly mean wind. It developed further in the next 6 h, but then broke up into several cloud clusters and covered a larger area by 8/15/06Z. Note that diurnal convection is also frequently observed over the

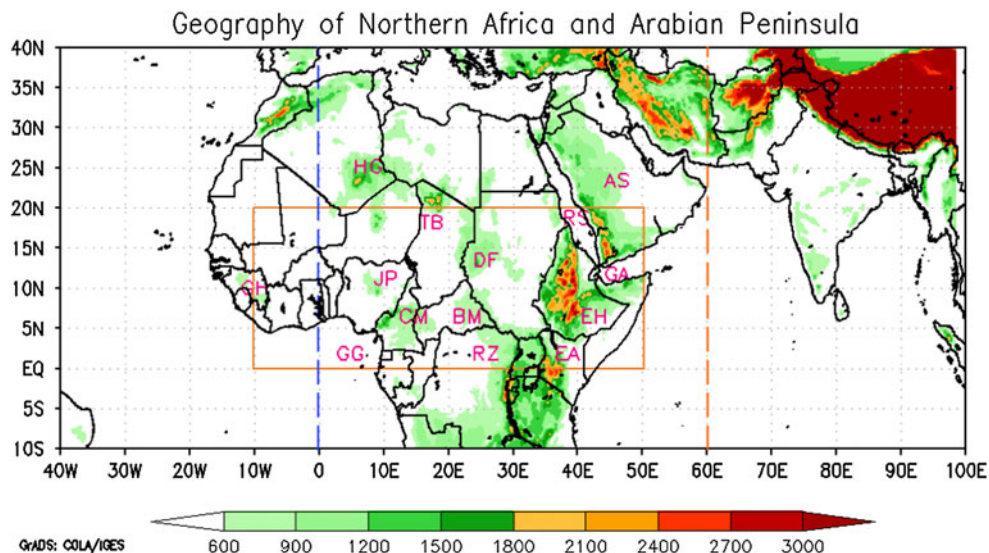


Fig. 2 Geography for Africa (north of 10°S) and southern Arabia Peninsula. Labels indicate major geographic features: AS Asir Mountains, BM Bongo Massif, CM Cameron Highlands, DF Darfur Mountains, EA Eastern Arc Mountains, EH Ethiopian Highlands, GH Guinea (Futa Jallon) Highlands, GA Gulf of Aden, GG Gulf of

Guinea, HG Hoggar Mountains, JP Jos Plateau, RZ Ruwenzori Mountains, TB Tibesti Mountains. The outer domain of the CNTL simulation is (40°W, 10°S) to (60°E, 40°N), while the inner domain of the CNTL case (8 km resolution) is enclosed by the brown lines. The domain of EAST simulation is from (0°, 10°S) to (100°E, 40°N)

Table 1 List of acronyms

Acronym	Meaning
AEW	African easterly waves
AP	Arabian Peninsula
ARW	Advance research WRF model
AEW-MCS	Coupled AEW and MCS system
AS	Asir mountains
AS-EH	Asir mountains and Ethiopian highlands region
CCC	Convective cloud cluster
DF	Darfur mountains
EH	Ethiopian highlands
GFS	Global forecast system
GH	Guinea (Futa Jallon) highlands
GRISAT	Grid satellite data
ITCZ	Inter-tropical convergence zone
JP	Jos plateau
MCS	Mesoscale convective system
MDR	Main development region (in Atlantic Ocean)
OLR	Outgoing longwave radiation
TC	Tropical cyclone
SM	Sarawat mountains (in southwest Arabian Peninsula)
WRF	Weather research forecast model

Table 2 List of ARW numerical experiments

Cases	Features
CNTL	Control experiment: Outer domain: (40°W, 10°S)–(60°E, 40°N); $\Delta x = 24$ km; 8/10/00Z–8/24/00Z Inner domain: (10°W, 0°)–(50°E, 20°N); $\Delta x = 8$ km; 8/11/12Z–8/18/00Z (see Fig. 2 for domain coverage)
EAST	Domain: (0°, 10°S)–(100°E, 40°N); $\Delta x = 24$ km; 8/1/00Z–8/16/00Z (similar to CNTL; see Fig. 2 for domain coverage)

highlands of central and western Africa, such as Air in West Niger, and Jos Plateau in North Nigeria, which tends to enhance the convective cloud clusters.

At 8/16/00Z, the cloud cluster C (Fig. 1b) over the DF at 8/15/12Z split into cloud clusters D and E. Cloud cluster D

dissipated during the period 8/16/00Z to 8/16/12Z thus became less identifiable, while cloud cluster E disappeared at 8/16/12Z. Note that a cloud cluster appeared near (2°–3°N, 20°E) might develop further and migrated northward and merged with cloud cluster D. However, cloud cluster D (Fig. 1b) appeared to go through the nocturnal convection over the DF. It grew stronger in the afternoon around 1400 local time (8/16/18Z), as can be clearly identified near (20°E, 10°N) and afterwards. Owing to its MCS characteristics, i.e., a complex of thunderstorms that became organized on a scale larger than the individual thunderstorms and persists for several hours (Houze 1993), and served as a precursor of Tropical Storm Debby (2006), this more-coherent cloud cluster formed after 8/16/18Z may be called “pre-Debby MCS”.

Based on the satellite imagery, the cloud-merging and splitting processes were quite common for propagating

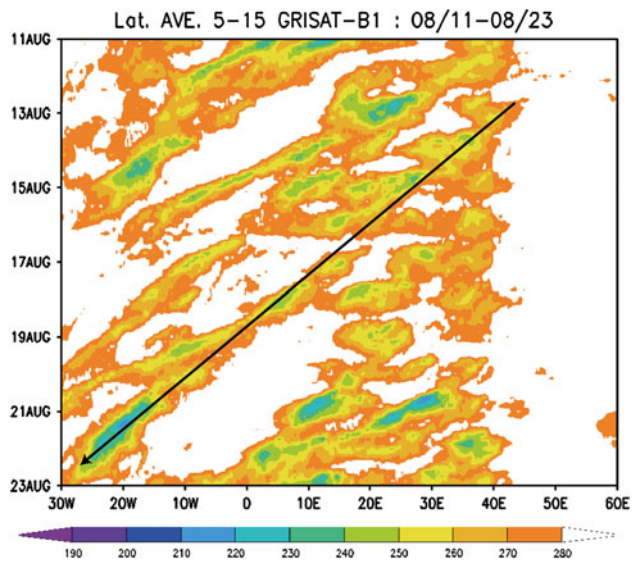


Fig. 3 Hovmoller diagrams of 5°–15°N averaged brightness temperature as observed from grid satellite (GRISAT) data. The *black straight line* denotes the approximate track of the pre-Debby MCS/convective cloud clusters

cloud clusters. The cloud-splitting process may be explained by the new cloud clusters developed at the gust fronts of the evaporative–cooling generated outward propagating density currents (e.g., Lin 2007). The left (westward) propagating density current, thus the left CCC, propagated westward faster with the addition of the easterly basic wind. In addition, the generation of new convective cells west of a pre-existing cloud cluster was favored by strong and dry easterly winds in the AEJ at ~ 600 – 700 hPa.

2.2 Evolution of the Pre-Debby MCS after 1800 UTC August 16

The pre-Debby MCS grew stronger from 8/16/18Z to around 8/17/06Z (Fig. 1b, c), went through splitting process in the next 12 h or so, and then continued to grow after 8/17/18Z until encountered the Guinea (Futa Jallon) Highlands (GH) around 8/19/12Z (Fig. 1c, d). Note that the propagating AEW and MCS/CCCs may be weakened or split by orographic blocking, but in the meantime they may be strengthened or weakened by the diurnal heating or cooling over the mountains. This may help explain the discontinuity of the pre-Debby MCS (e.g., Lin et al. 2005). The relative strength of these forcing depends on several factors, which may be represented by the orographic Froude number (U/Nh , where U is the mean wind speed, N the buoyancy frequency and h the mountain height) and the thermal Froude number (U/Nd , where d is the heating or cooling height) (see Lin 2007, p. 195). This deserves a separate study.

The propagation of pre-Debby MCS D from 8/16/18Z to the Atlantic Ocean was smooth except when it approached GH. During its passage over GH, it appeared that convection developed quicker on the lee and southern sides of the mountains during the period 8/20/00Z to 8/20/06Z. Before the splitting process occurred over GH on 8/20/06Z, the pre-Debby MCS showed a binary structure with different evolution of its northern and southern parts. At 8/20/06Z, the pre-Debby MCS D split into cloud clusters D and E. The downstream cloud cluster E continued to propagate westward, while the upstream cloud cluster D regrouped and developed into a stronger MCS (Fig. 1d). This MCS then triggered the Tropical Storm Debby over the ocean after 8/21/00Z. This splitting process over the GH is clearly depicted in the Hovmoller diagram of the brightness temperature analyzed from the GRISAT (Fig. 3). The pre-Debby MCS D propagated at a speed approximately 7.4 ms^{-1} of speed during the period 8/16/18Z to 8/21/18Z, near the lower end of climatological mean speed of 7 – 9 ms^{-1} (Reed et al. 1977) but comparable to that of pre-Alberto (2000) MCS (Lin et al. 2005).

2.3 Upstream environments of the Pre-Debby cloud clusters and AEW

Owing to the lack of observational data over eastern Africa, the upstream environments for the pre-Debby cloud clusters and AEW are examined by using the GFS analysis data. Using the cloud water content data, three to four convective cloud clusters co-existed along the belt of 5°–15°N, which are associated with the ITCZ (Fig. 5), prior to the pre-Debby MCS can be traced back to EH-AS region and Arabian Peninsula (Fig. 4). In Fig. 4, it can be seen that there were convective clouds over Arabian Sea, but not much convective cloud activities shown over the southern coast of Arabian Peninsula. This seems consistent with the cutoff of cloud water contents east of EH-AS region in the Hovmoller diagram (Fig. 12a).

The pre-Debby MCS/cloud cluster can be approximately traced back to about 42°E, just over AS and the eastern edge of EH, by the Hovmoller diagram of the ARW simulated 5°–15°N averaged cloud water contents (Fig. 6). Note that the pre-Debby MCS analyzed by the GFS (Fig. 4) and simulated by ARW (Fig. 6) moved faster than that analyzed in the satellite imagery and GRISAT data (Figs. 1, 3). Based on the GRISAT data (Fig. 3), GFS data (Fig. 4) and ARW simulation (Fig. 6), and NOAA Climate Prediction Center (CPC) Famine Early Warning System (FEWS) net rainfall estimate (Fig. 5), it appears that the cloud clusters prior to the pre-Debby MCS were originated over EH-AS region and downstream (west) of it. To trace the origins of the pre-Debby (2006) MCS/cloud clusters, as well as the pre-Debby AEW, we will perform regional

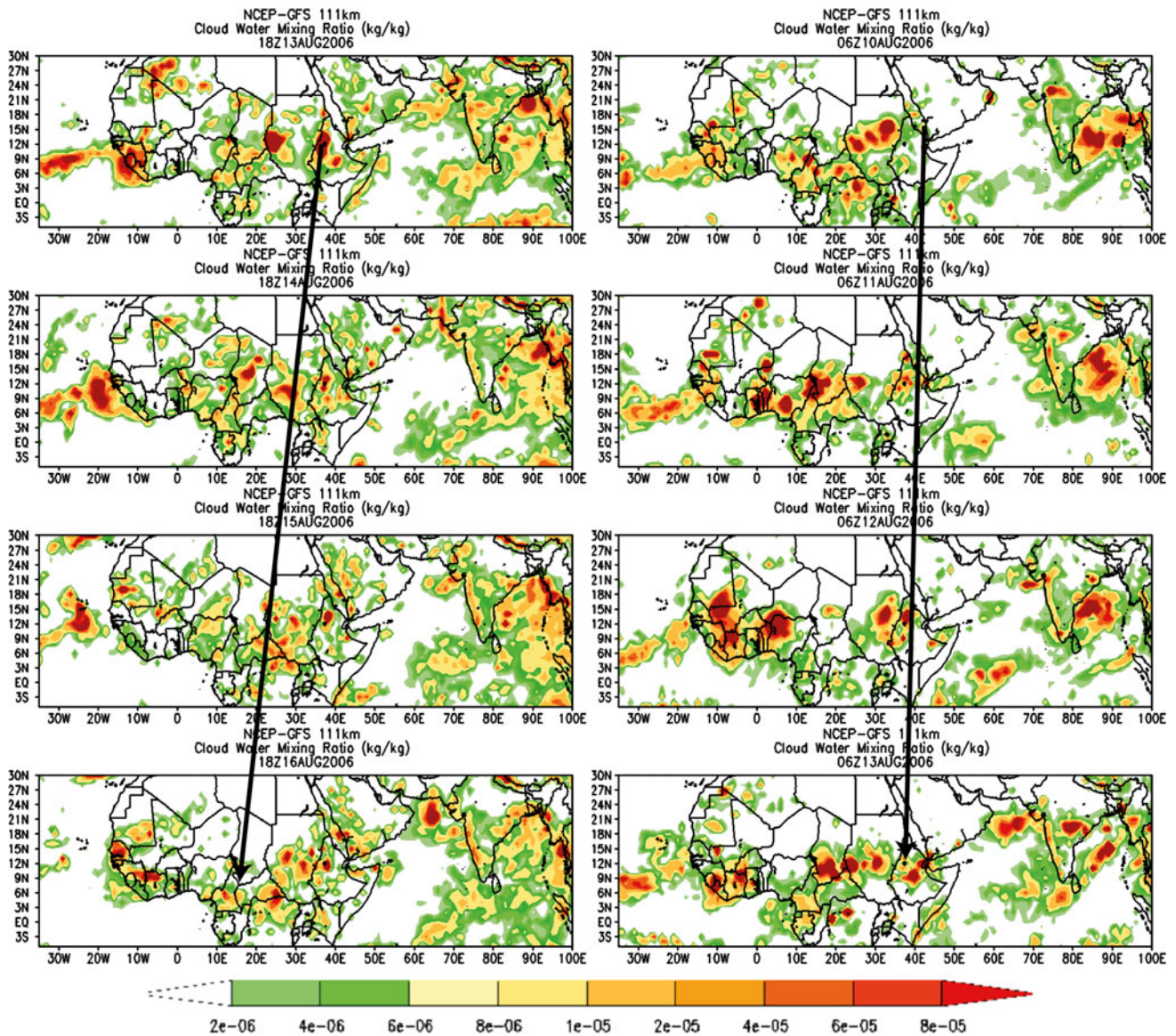


Fig. 4 Atmospheric column cloud water mixing ratio (kg kg^{-1}) from GFS analysis data every 24 h for the periods of 8/10/06Z to 8/13/06Z and 8/13/18Z to 8/16/18Z 2006. The arrows denote approximately the pre-Debby (2006) MCS or convective cloud clusters

modeling simulations using ARW. The model description and experimental design can be found in the “Appendix”.

3 Origins of Pre-Debby MCS and AEW and their precursors

3.1 Origins of pre-Debby MCS and its precursors

A comparison between GRISAT data and ARW results (Figs. 3, 6) reveals that the observed population of MCSs is more complex than the simulated one. However, the quasi-continuous nature of convective activities of the cloud clusters prior to the pre-Debby MCS can also be seen in the

Hovmöller diagram of the OLR field (Fig. 6). Note that the ARW simulated pre-Debby MCSs, as well as the pre-Debby AEW, forms earlier and propagates much faster than the observed one due to a more continuous OLR envelope. The diurnal convection over EH and DF can be seen clearly in this Hovmöller diagram. The advection, splitting, and merging processes among the convective cloud clusters mentioned above can be seen clearly from the figure. The OLR field simulated by the CNTL case is also consistent with the cloud water mixing ratio field, which is equivalent to the OLR field, as shown in Fig. 11a (to be discussed later). The local OLR minima, as denoted by the concentrated red and blue areas in the horizontal belt centered on 10°N (Fig. 7), are used as a proxy of MCS or

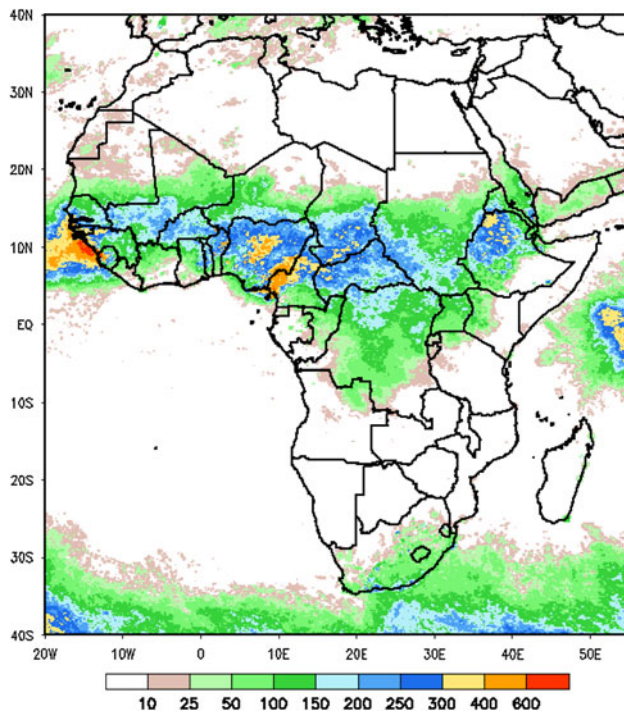


Fig. 5 The NOAA Climate Prediction Center (CPC) Famine Early Warning System (FEWS) net rainfall estimate (mm) for the Northern Africa rainfall climatology for the month of August 2006 (NOAA 2006)

cloud clusters, which compare reasonably well with the locations of the pre-Debby CCCs and MCS (Fig. 1). In general, the ARW model is able to capture major features of the pre-Debby MCS/cloud clusters and AEW from observations. The cloud clusters over northern EH, Red Sea, and AS (EH-AS region) (Fig. 1a) are captured by the model at 8/11/06Z (upper right panel of Fig. 8).

3.2 Origins of the pre-Debby AEW and its precursors

The pre-Debby (2006) AEW and its precursor can be traced by localized cyclonic relative vorticity maximum using ARW-simulated relative vorticity fields (Figs. 6, 9) back to 35°E, approximately over the EH, which are collocated with the observed and ARW-simulated pre-Debby MCS or cloud clusters (Figs. 1, 3, 6, 7, 8). The simulated AEW or vorticity perturbations of the CNTL case (Fig. 9) is also consistent with the GFS analysis data (Fig. 10), which appear to be from about 35°E over the western EH at 8/12/06Z more firmly and to southern Arabian Peninsula around 48°E less firmly. To make sure about the origin of the pre-Debby AEW, a Hovmoller diagram of the relative vorticity averaged over 10°–20°N and 700–500 mb from GFS analysis data for the period of 8/2/00Z to 8/16/00Z was plotted (Fig. 11b). The approximate track of the local positive vorticity maximum can be traced back to southern

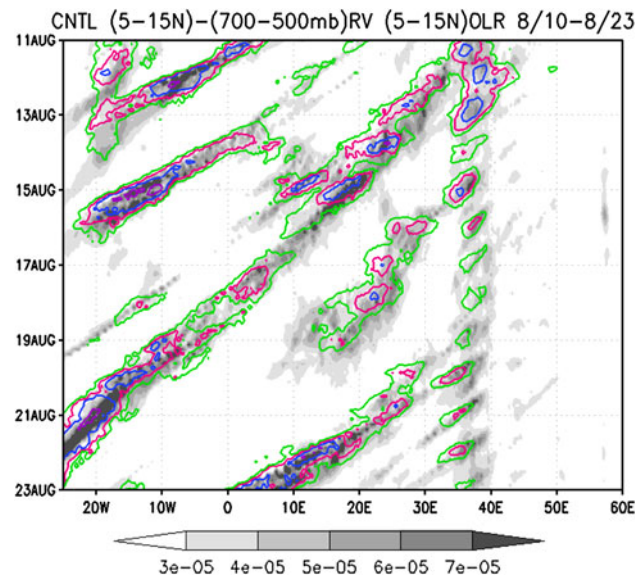
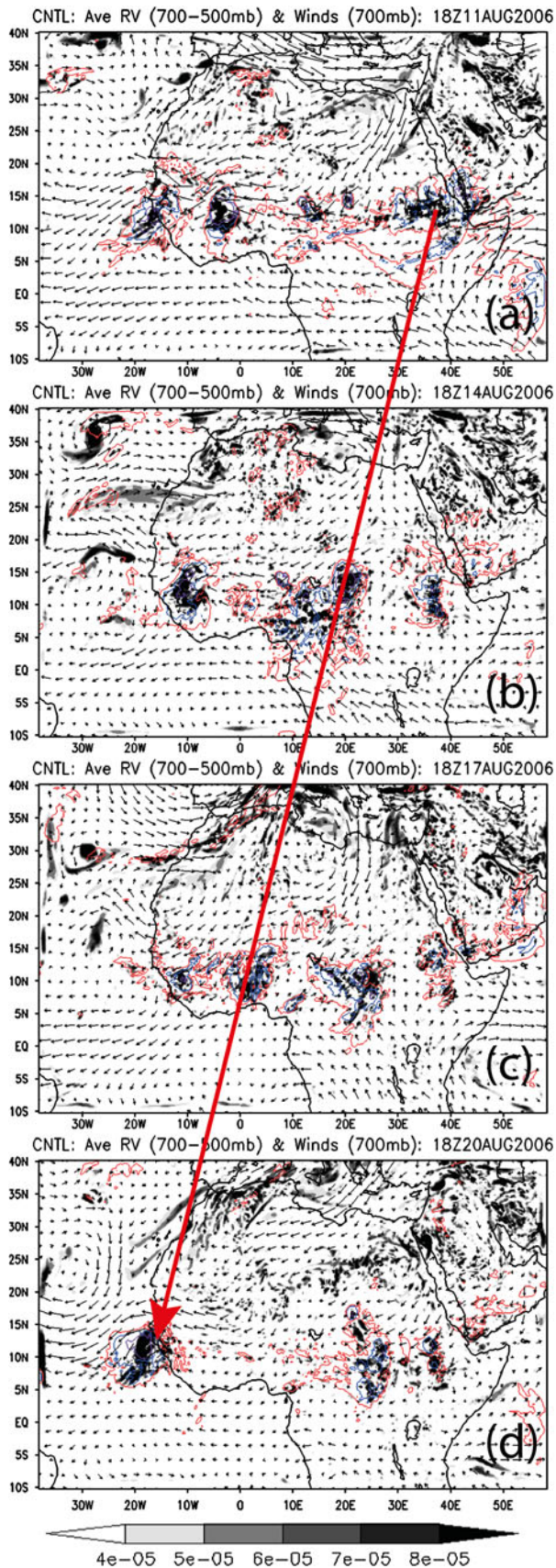


Fig. 6 (Case CNTL): Hovmoller diagrams for the averaged 5°–15°N OLR (contour) and averaged 700–500 mb and 5°–15°N relative vorticity (s^{-1}) (shaded) simulated by the 24 km resolution ARW model for case CNTL

Arabian Peninsula and Arabian Sea ($\sim 48^\circ E$). Note that the Hovmoller diagrams of cloud water mixing ratio from satellite imagery (Fig. 3), GFS data (Figs. 4, 11a) and CNTL case (Figs. 6, 7, 8) also show that the pre-Debby (2006) convective cloud clusters were originated from southern Arabian Peninsula near 43°E.

To explore this, we performed a case (Case EAST), similar to case CNTL but with the domain shifted eastward from 0° to 100°E (Fig. 2) and the integration time from 8/1/00Z to 8/16/00Z. Based on the case EAST, the Hovmoller diagram of OLR (Fig. 12a) corresponds roughly to the cloud water mixing ratio plot of Fig. 11a, which indicate that the pre-Debby convective cloud clusters was originated around 43°E (Figs. 10, 11a), while the Hovmoller diagram of the cyclonic (positive) vorticity perturbation or the precursor of the pre-Debby AEW was originated slightly to the east around 50°E (Fig. 12b) at approximately 8/10/18Z. Note that relative vorticity at 40°E is close to 0, which is attributed the obstruction of the Ethiopian Highlands, as revealed in one of our sensitivity experiments (not shown). In addition, the strong relative vorticity at 70°–90°E is due to the storm crossing Indian subcontinent (Figs. 13, 14). Although their origins are slightly different, basically they were formed around the same region, i.e. the Sarawat Mountains in southwest Arabian Peninsula, as can be seen from the OLR (Fig. 13) and relative vorticity (Fig. 14) at 8/10/18Z.

Based on ARW simulated OLR field of case EAST, we are able to trace the pre-Debby MCS or convective cloud cluster back to the southwest Arabian Peninsula near 43°E



◀ **Fig. 7** (Case CNTL): the outgoing longwave radiation (OLR, *color-contoured*), 700-mb horizontal wind vector, and 500–700 mb averaged relative vorticity (*gray shaded*, in s^{-1}) fields simulated by the ARW model with 24 km resolution for Case CNTL. *Contours* for OLR are: *red* for 220 K, *blue* for 130 K, and *purple* for 95 K. The MCS-AEW system is denoted by the *red arrow line*

around 8/10/18Z. Note that the ARW simulated pre-Debby convective cloud clusters formed earlier and propagated faster than the observed cloud clusters. For example, the pre-Debby MCS was located at (20°E, 10°N) at 8/16/18Z, which was located at the same location, but around 8/15/00Z. Before then, there were no noticeable signatures of CCCs (not shown). In fact, this CCC was part of the ITCZ which normally exists in August along the southern Arabian Peninsula (Fig. 5). This cloud cluster was moving downstream with the northeasterly wind to EH (~40°E) at later time around 8/11/18Z. At this time, the pre-Debby cloud cluster was strengthened by the orographically induced diurnal convective cloud cluster over EH, which kept moving westward until around 8/16/18Z when it can be clearly identified as pre-Debby (2006) MCS, consistent with that of case CNTL (Fig. 6) and GFS analysis data (not shown). Thus, the convective cloud clusters preceding the pre-Debby MCS were originated from the southwest Arabian Peninsula near ITCZ around 8/10/18Z. Figure 14 shows the evolution of ARW model simulated relative vorticity field with time for case EAST. The cyclonic vorticity perturbation preceding the pre-Debby AEW can also be traced back to the same location and time, i.e. southwestern Arabian Peninsula near the ITCZ around 8/10/18Z.

3.3 Sources of cyclonic vorticity and convective cloud clusters preceding the pre-Debby AEW-MCS system

The low-level wind fields at 700 mb (Fig. 13) and at 900 mb (Fig. 14) suggest that the convective cloud clusters and the cyclonic vorticity perturbations were produced by the cyclonic convergence of the northeasterly wind burst toward the southwestern Arabian Peninsula and the Somali jet, as part of the southwesterly monsoon current associated with the Indian Ocean High, right before 8/10/18Z. Note that the Somali jet is stronger in the lower layer, such as 900 mb, while the northeasterly wind burst is stronger at the 700 mb than at 900 mb. The northeasterly wind appears to be related to the outbreak of summer “*Shamal*”. A *Shamal* is a northwesterly or northerly wind blowing over Iraq, Iran, and Saudi Arabia toward Arabian Sea, which is associated with a low over Iran and a high over eastern Mediterranean (e.g., Rao et al. 2003). The strengthening of the Iranian low and the Mediterranean high, and the southeastward extension of the pressure ridge

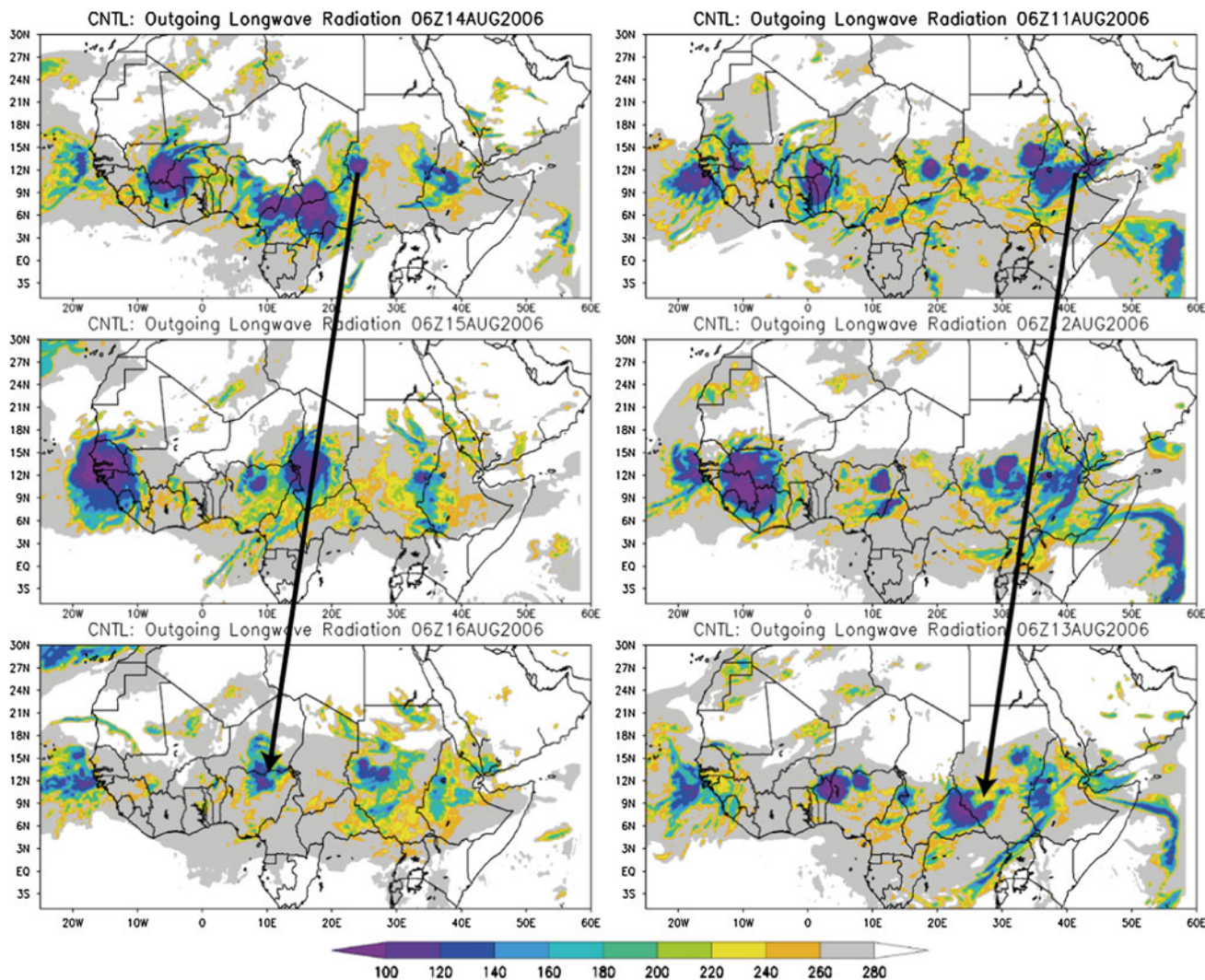


Fig. 8 (Case CNTL): the outgoing longwave radiation (OLR) fields for every 24 h starting from 8/11/06Z to 8/16/06Z 2006 simulated by the 24 km resolution (*outer domain*) ARW model. The approximate

positions of convective cloud clusters preceding the pre-Debby MCS is denoted by *long arrows*

from the high tend to generate the outbreak of summer Shamal. Occasionally, Shamal blows southwestward and interacts with the southwesterly Somali jet to produce a positive vorticity ($\zeta > 0$). The production of cyclonic vorticity can be explained by the approximate vorticity equation for synoptic (large-scale) flow,

$$\frac{\partial \zeta}{\partial t} = \left(-u \frac{\partial \zeta}{\partial x} - v \frac{\partial \zeta}{\partial y} - w \frac{\partial \zeta}{\partial z} \right) - (\zeta + f) \left(\frac{\partial u}{\partial x} + \frac{\partial v}{\partial y} \right). \quad (1)$$

The above equation indicates that the local rate of change of relative vorticity ($\partial \zeta / \partial t > 0$) may increase mainly through the vorticity advection and/or the convergence of the convergence term of the vorticity equation ($-(\zeta + f)(\partial u / \partial x + \partial v / \partial y)$). The tilting term normally plays a minor role in synoptic scale flow (e.g., Holton 2004). In the current situation, the generation of local

cyclonic (positive) vorticity is mainly due to the positive vorticity convergence. The vorticity advection plays a less significant role since no major positive vorticity exists upstream of this area. The convergence also helps strengthen the convection associated with ITCZ, which, in turn, increases the relative vorticity through vorticity stretching since the second term on the right side of (1) can be written as $(\zeta + f)w$. The cyclonic convergence zone is situated along the coast of Arabian Sea in the vicinity of the ITCZ and coincided approximately with the general location of ITCZ in August (Fig. 5).

The cyclonic (positive) vorticity perturbations, as shown in the north–south Hovmoller diagram averaged over 40°–50°E and 700–500 mb (Fig. 15c) were associated with the northeasterly wind burst and Somali jet as can be seen in the north–south Hovmoller diagram of the U wind (Fig. 15a)

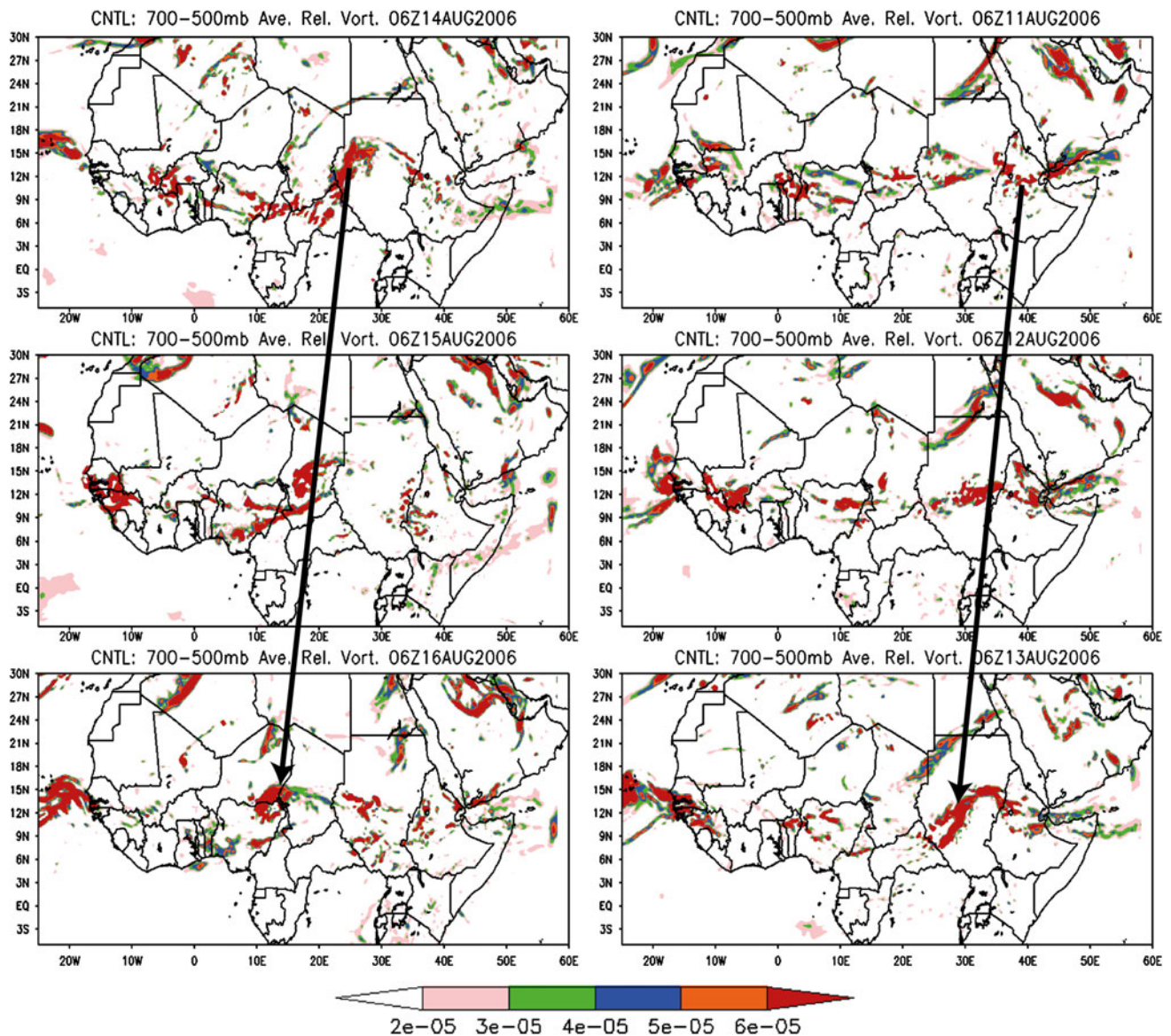


Fig. 9 (Case CNTL): the averaged 500–700 mb cyclonic relative vorticity (shaded, in s^{-1}) and vector wind fields based on the 24 km resolution (*outer domain*) ARW simulated results for every 24 h starting from 8/11/06Z to 8/16/06Z. The relative vorticity areas higher

than $2.0 \times 10^{-5} s^{-1}$ are shaded. The black arrows denote the propagation of the pre-Debby AEW and its precursor (cyclonic vorticity perturbation)

and the east–west Hovmoller diagram of the V component of the wind (Fig. 15f). Figure 16a and f also indicate that in this area the generation of cyclonic vorticity is dominated by the U component of the wind ($-\partial u/\partial y$) (Fig. 15a) than the V component of the wind ($\partial v/\partial x$) (Fig. 15f). An interesting and important feature of the U component of the wind in this region (40° – 50° E) is the southward advection of the cyclonic (positive) vorticity perturbations in three time periods started around August 3, 7, and 11 (Fig. 15a–c). Apparently, these cyclonic vorticity perturbations were generated by the interaction between the northeasterly wind bursts and the Somali jet (Fig. 15b, e, f).

The cyclonic vorticity was generated approximately every 4 days, which might dictate the time interval between AEWs downstream (to the west) over central and western North Africa (Fig. 6). The third cyclonic vorticity perturbation started around 8/11/06Z near southwest Arabian Peninsula eventually evolved into the pre-Debby AEW downstream of northern EH ($\sim 38^{\circ}$ – 40° E) as denoted by the long arrow in Fig. 9. Unlike the pre-Debby MCS which can only be identified clearly from satellite imagery starting at 8/16/18Z, the pre-Debby AEW can be traced by cyclonic vorticity perturbation almost continuously back to 8/11/06Z (Figs. 6, 9, 10, 14).

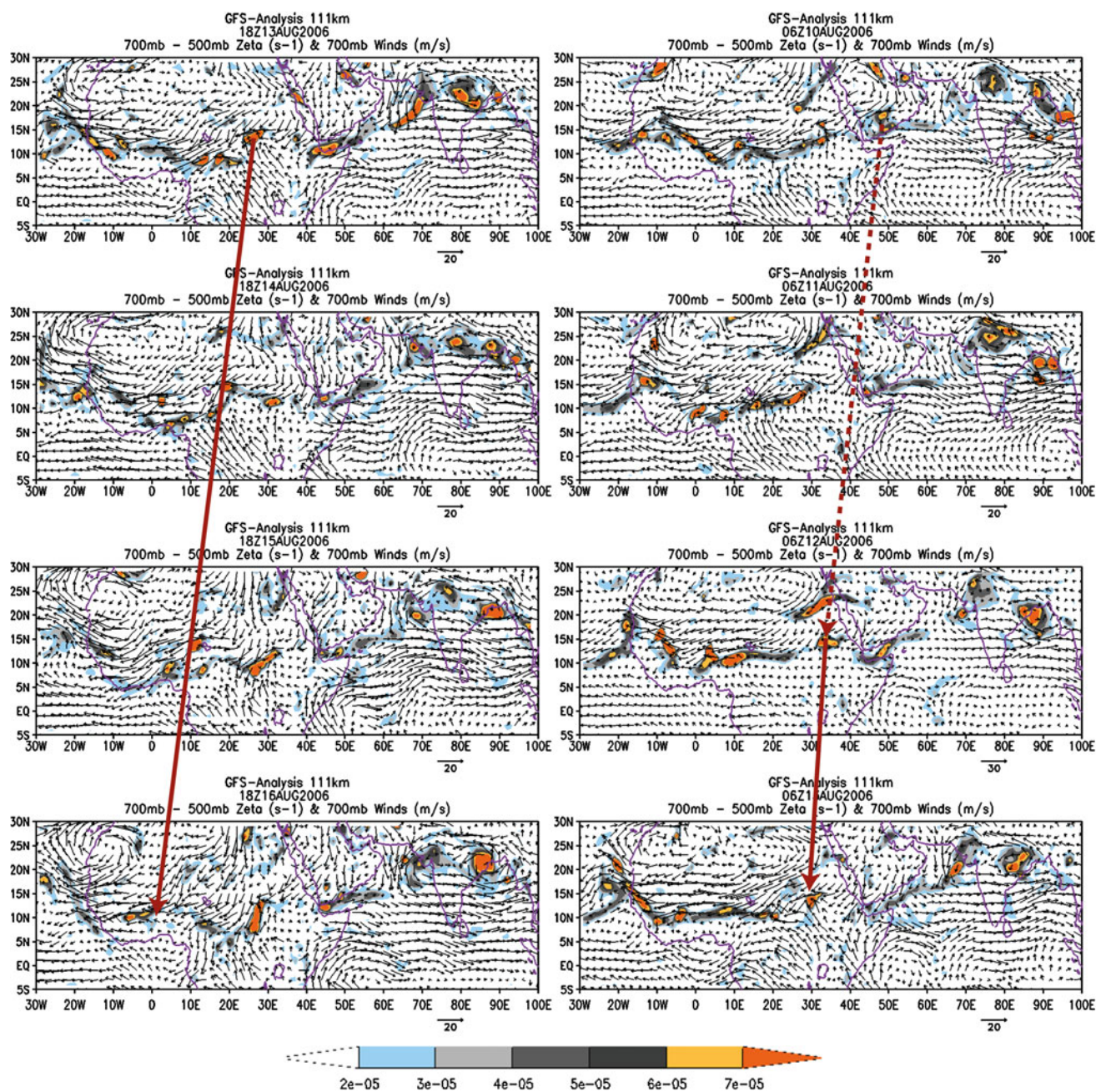


Fig. 10 The 700–500 mb averaged relative vorticity and 700 mb wind vectors from GFS analysis data every 24 h for the periods of 8/10/06Z to 8/13/06Z and of 8/13/18Z to 8/16/18Z. The red solid

(dashed) line denotes the approximate (possible) track of pre-Debby AEW/vorticity perturbation

The formation of convective cloud clusters in southern Arabian Peninsula during this period (August 2–16) (Fig. 15d) occurred around the same times as those of the cyclonic vorticity perturbations (Fig. 15c), i.e. August 3, 7, and 11. This implies that the formation of convective cloud clusters is related to that of cyclonic vorticity perturbations which were driven by the interaction between the northeasterly wind burst and Somali jet, as shown in the north-south Hovmöller diagrams of the 40°–50°E averaged U and

V wind components (Fig. 15a, b). The convective cloud clusters were developed first within the ITCZ and then followed by the development of MCS. As noted earlier, the convective cloud clusters were generated by the convective heating associated with ITCZ, while the cyclonic vorticity was generated by the cyclonic convergence as shown in the U component of the horizontal wind (Fig. 15a).

To explore the synoptic scale environment conducive to the formation of the cyclonic vorticity perturbations and

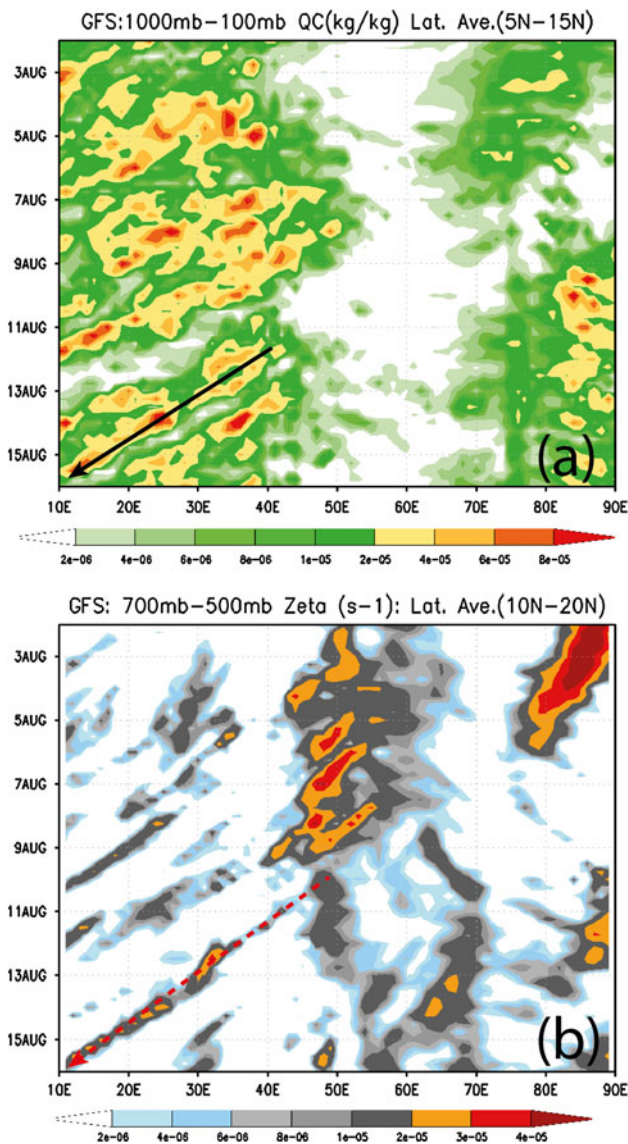


Fig. 11 (GFS): Hovmoller diagrams for **a** cloud water mixing ratio (kg kg^{-1}) averaged over $5^{\circ}\text{--}15^{\circ}\text{N}$ and **b** relative vorticity (s^{-1}) averaged over $10^{\circ}\text{--}20^{\circ}\text{N}$ and 700–500 mb from the GFS data

convective cloud clusters preceding the pre-Debby AEW–MCS system, we plotted event and non-event composite fields for cyclonic vorticity perturbations and convective cloud clusters in the vicinity of the southwest Arabian Peninsula (Fig. 16). Based on the OLR, positive relative vorticity, and 700 mb vector wind fields of case EAST, similar to the plots of Figs. 13 and 14, the following event dates are selected: 8/2/18Z, 8/5/18Z, 8/7/18Z, and 8/11/18Z, while the non-event dates selected are: 8/4/06Z, 8/8/06Z, 8/9/06Z, and 8/10/06Z. During the event, the Indian Ocean high was strong and its associated Somali jet penetrated farther to the north along the coast of Arabian sea, and interacted with the northeasterly Shamal to produce strong convergence and cyclonic vorticity there.

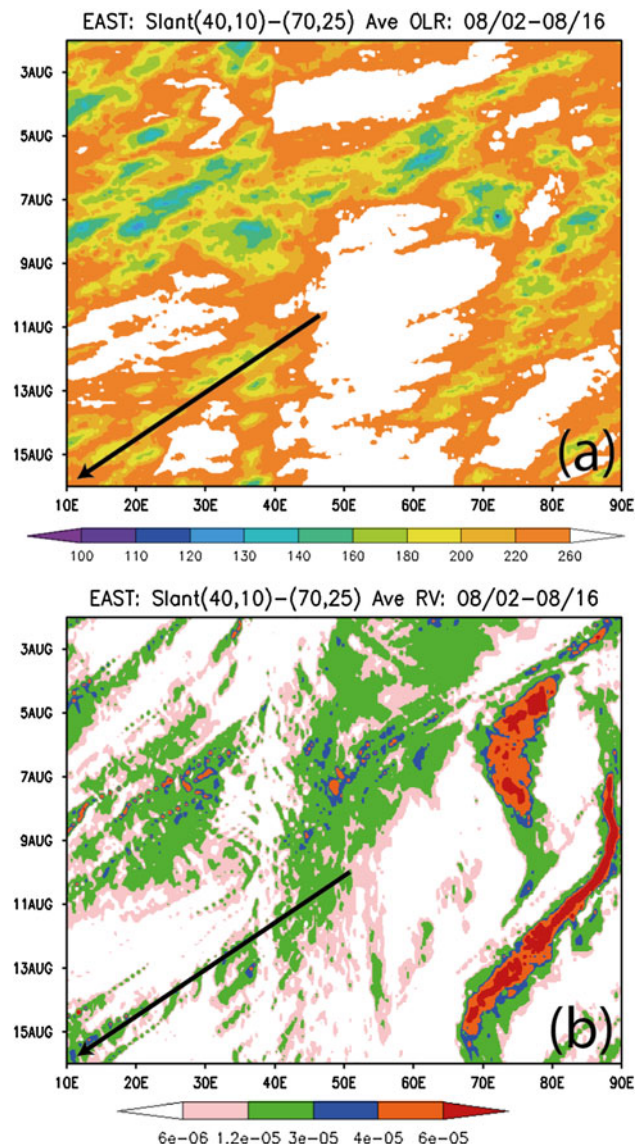


Fig. 12 (Case EAST): Hovmoller diagrams for **a** OLR and **b** relative vorticity (s^{-1}) averaged over 700–500 mb, $5^{\circ}\text{--}15^{\circ}\text{N}$ to the west of 40°E and $20^{\circ}\text{--}30^{\circ}\text{N}$ to the east of 70°E , and over a 10° band along a line from $(40^{\circ}\text{E}, 10^{\circ}\text{N})$ to $(70^{\circ}\text{E}, 25^{\circ}\text{N})$ (approximately along the southern Arabian Peninsula), as simulated by the 24 km resolution ARW model for case EAST

4 Concluding remarks

Based on the analysis of the Meteosat-8 infrared imagery and GRISAT data, the pre-Debby (2006) MCS was clearly traced back to 8/16/18Z near $(20^{\circ}\text{E}, 10^{\circ}\text{N})$, which was formed by a series of successive, more or less organized cloud clusters during the period 8/11/00Z to 8/16/18Z. These cloud clusters developed over the area of southwest Arabian Peninsula, Asir Mountains, and Ethiopian Highlands. During this period, the convective cloud clusters went through growing, splitting, advection, weakening, and merging processes, then propagated westward across the

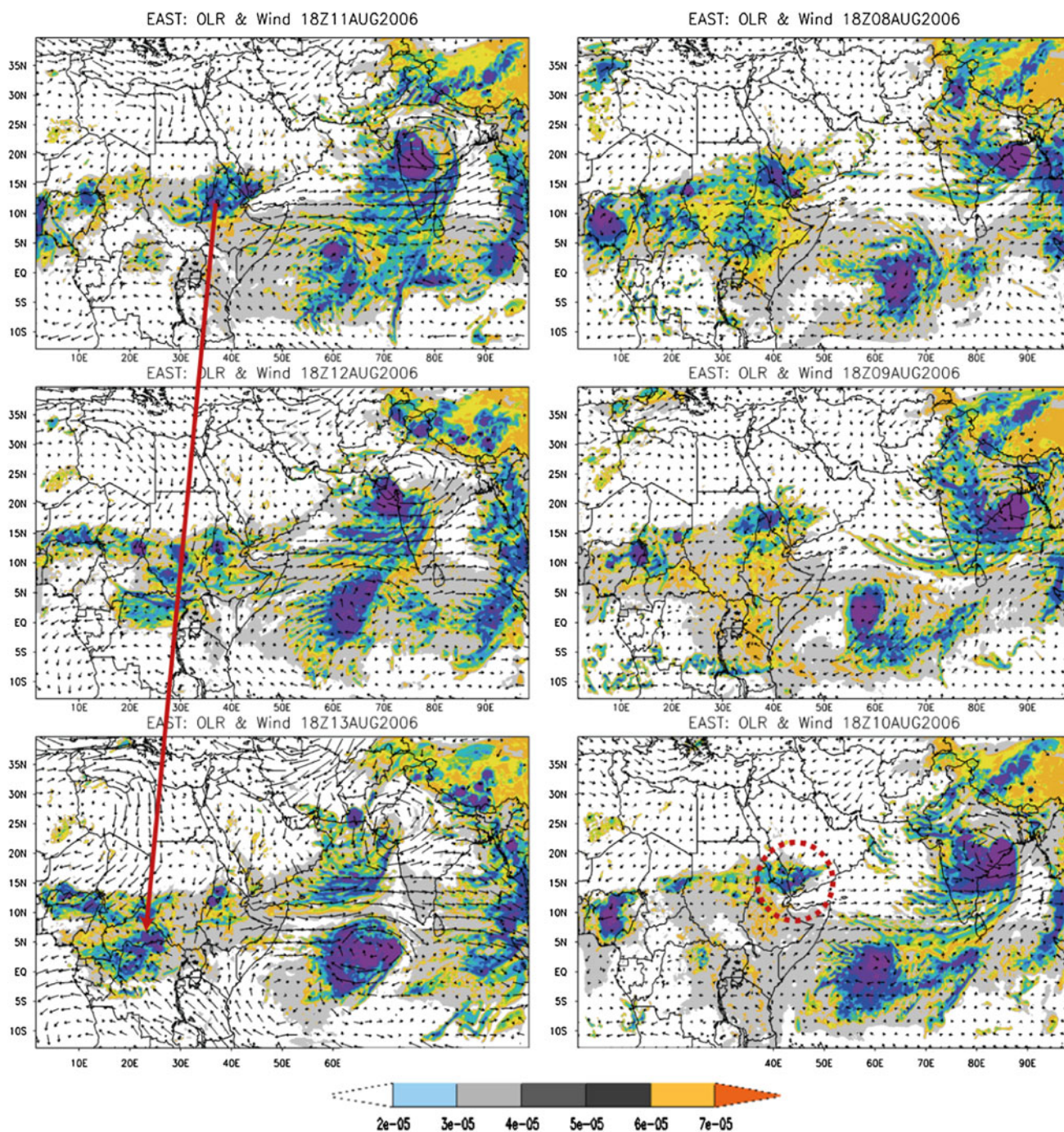


Fig. 13 (Case EAST): the OLR (outgoing longwave radiation) and 700 mb vector wind fields of Case EAST based on the 24 km resolution ARW simulated results for every 24 h from 8/8/18Z to

8/13/18Z. The location of the precursor of pre-Debby MCS is denoted by a *dashed circle* at 8/10/18Z and by a *long arrow line* afterwards

North African continent at later times. During these processes, not every individual cloud cluster survived. In fact, some of them propagated faster than the average speed and dissipated while a new MCS or cloud cluster formed. Some of the propagating MCS/cloud clusters and AEW/vorticity perturbations were weakened or split by orographic blocking, but were strengthened or weakened by the

diurnal heating or cooling over the mountains. This may help explain the discontinuity of the pre-Debby MCS/convective cloud clusters. When the pre-Debby MCS passed over GH, the convection developed quicker on the lee and southern sides of the mountains during the period 8/20/00Z to 8/20/06Z. At 8/20/06Z, the pre-Debby MCS split into two cloud clusters, as revealed by the GRISAT

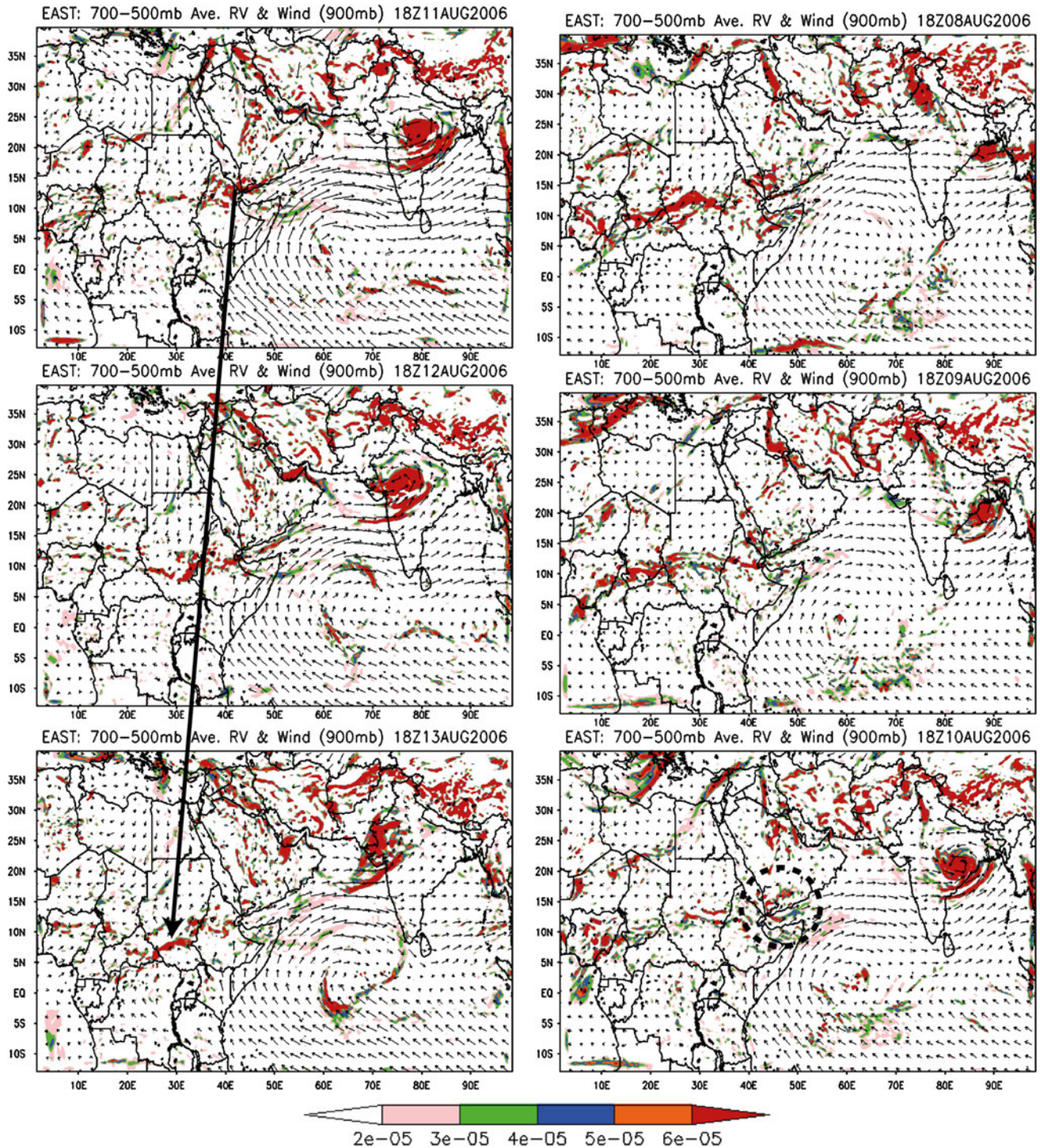


Fig. 14 (Case EAST): the cyclonic relative vorticity averaged over 500–700 mb and the 900 mb vector wind fields of Case EAST based on the 24 km resolution ARW simulated results for every 24 h from

8/8/18Z to 8/13/18Z. The location of the precursor of pre-Debby AEW is denoted by a *dashed circle* at 8/10/18Z and by a *long arrow line* afterwards

data. The downstream cloud cluster continued to propagate westward, while the upstream cloud cluster regrouped and developed into a stronger MCS which then triggered the Tropical Storm Debby (2006) over the ocean after 8/21/00Z. The propagation speed of the pre-Debby MCS during

the period 8/16/18Z to 8/21/18Z was slightly faster than the lower end of the climatological mean speed.

Using the GFS data, the pre-Debby cloud clusters was traced back to about 42°E, over EH-AS region and Arabian Peninsula. Three to four convective cloud clusters co-

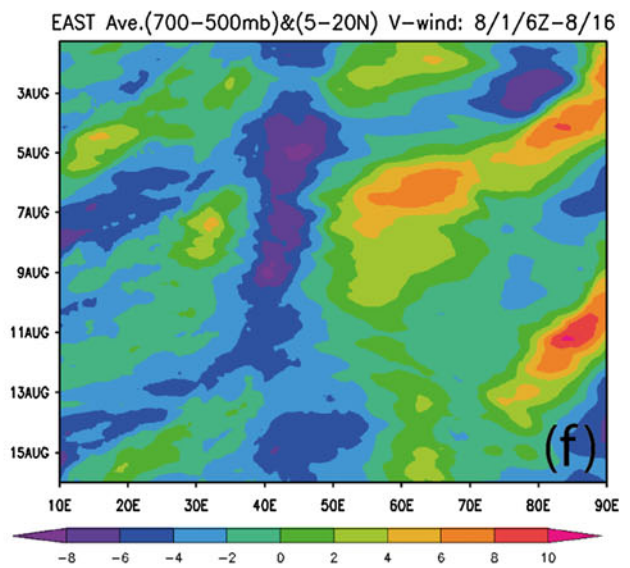
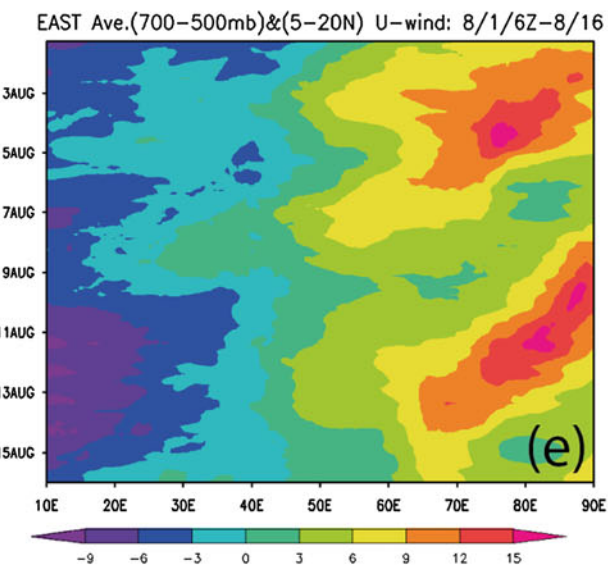
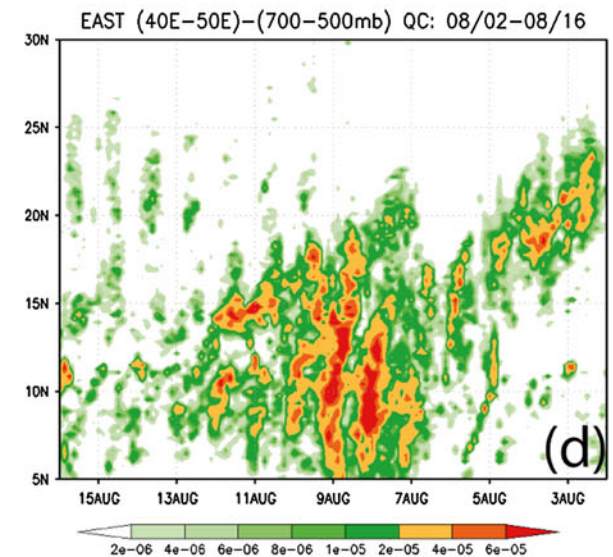
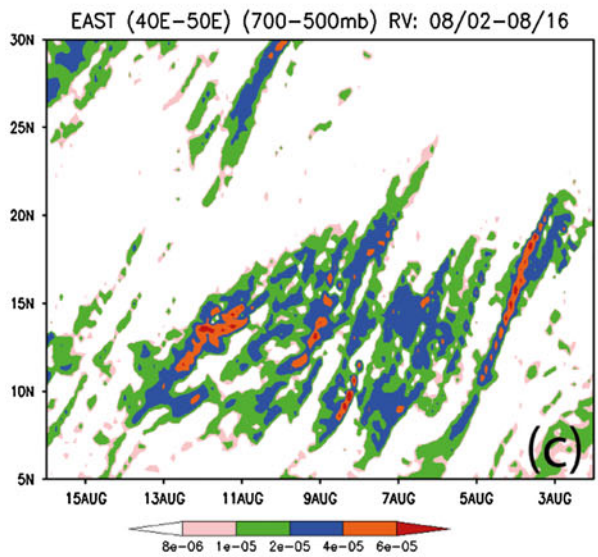
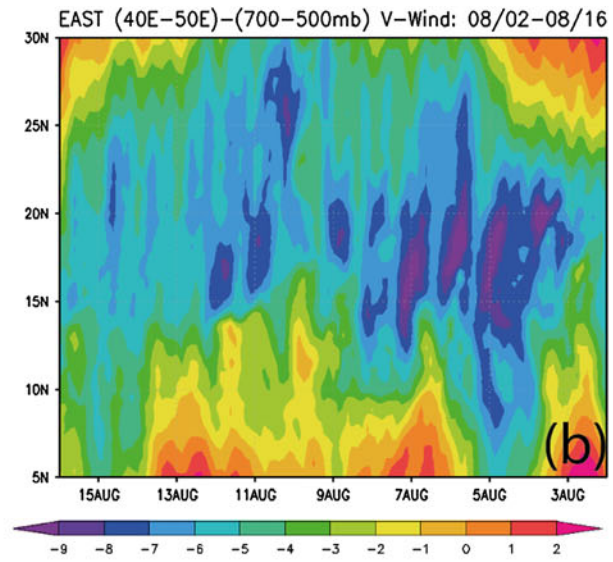
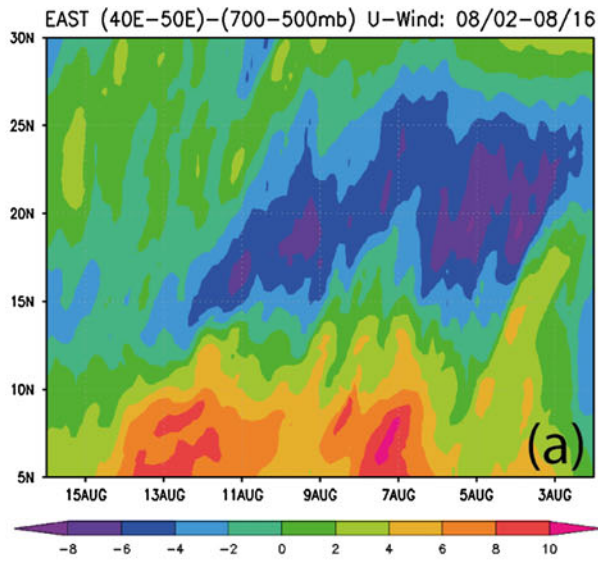


Fig. 15 (EAST): north–south Hovmoller diagrams based on ARW-simulated EAST case for 8/2/00Z to 8/16/00Z: **a** U wind (ms^{-1}), **b** V wind (ms^{-1}), **c** cyclonic (positive) relative vorticity (s^{-1}), and **d** cloud water mixing ratio (kg/kg) averaged over 40° – 50° E and 700–500 mb. **c, d** The same as **a** and **b**, but for east–west Hovmoller diagrams of 5° – 20° N and 700–500 mb averaged U and V, respectively

existed along the belt of $5\text{--}15^{\circ}\text{N}$, which were associated with the ITCZ. The ARW simulation (case CNTL) was able to capture the pre-Debby MCS/cloud clusters as observed in the satellite imagery and GFS analysis data for the period 8/11/00Z to 8/16/18Z except discrepancies existed in their intensity, timing of occurrence and dissipation, and faster propagation speed. The simulated pre-Debby cloud clusters went through growth, splitting, weakening, and merging processes, and were traced to the

area surrounding EH-AS region. The simulated diurnal convection over EH and DF can be seen clearly from this Hovmoller diagram. The ARW-simulated relative vorticity fields indicated that the pre-Debby AEW or cyclonic vorticity perturbation was originated around 50°E around 8/10/18Z in southwest Arabian Peninsula in the vicinity of the ITCZ near the Sarawat Mountains, slightly to the east of the origin of the pre-Debby cloud clusters, at 8/10/18Z.

It was found that the convective cloud clusters and the cyclonic vorticity perturbations were produced by the cyclonic convergence of the northeasterly wind burst toward the southwestern Arabian Peninsula and the Somali jet right before 8/10/18Z. The northeasterly wind might be related to the outbreak of “*Shamal*” wind, which was associated with the strengthening of the Iranian low and the southeastward extension of the pressure ridge from the

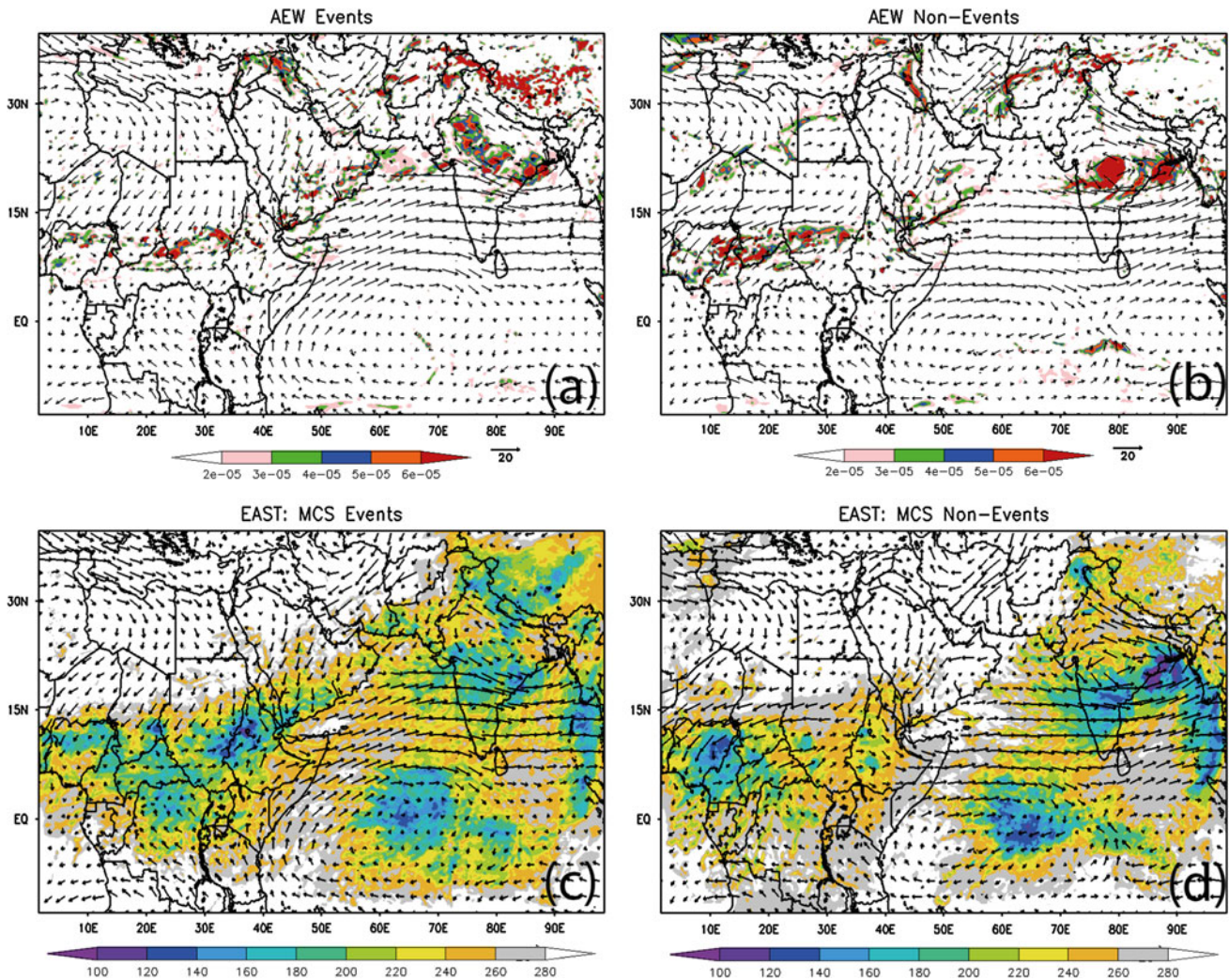


Fig. 16 Composite 700 mb vector wind, 700–500 mb average cyclonic (positive) vorticity, and OLR fields for pre-Debby (2006) AEW event **(a)** and non-event **(b)**, and for pre-Debby (2006)

convective cloud clusters event **(c)** and non-event **(d)**. Event is defined as the occurrence of AEW or convective cloud clusters over southwest Arabian Peninsula

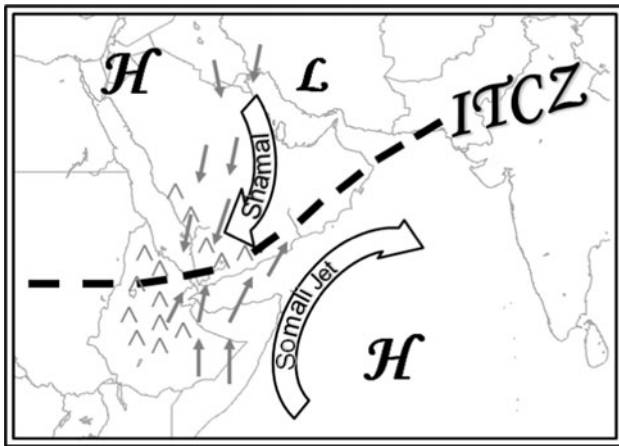


Fig. 17 A conceptual model of the generation of cyclonic vorticity perturbations and convective cloud clusters preceding the pre-Debby (2006) AEW–MCS system. The sources of the convective cloud clusters and vorticity perturbations were attributed to the cyclonic convergence of northeasterly Shamal wind and the Somali jet, especially when the Mediterranean High shifted toward east with high pressure ridge extended farther to the southeast and the Indian Ocean high strengthened and its associated Somali jet penetrated farther to the north. The cyclonic vorticity perturbations were strengthened by the vorticity stretching associated with convective cloud clusters and the convective cloud clusters are strengthened by the diurnal convection over the Sarawat Mountains, Asir Mountains, Ethiopian Highlands, and Darfur Mountains downstream of the genesis region—southwest Arabian Peninsula

Mediterranean high. The northeasterly Shamal appeared to interact with the southwesterly Somali jet to produce a cyclonic vorticity ($\zeta > 0$), which in turn increased the rate of change of relative vorticity through the convergence term of the vorticity equation. The cyclonic convergence zone is situated along the coast of Arabian Sea in the vicinity of the ITCZ. The argument was supported by the analyses of east–west Hovmoller diagrams of U and V components of the wind, and relative vorticity and cloud water mixing ratio, and north–south Hovmoller diagrams of U and V components of the wind. In addition, it was found that the cyclonic vorticity was generated approximately every 4 days, which might dictate the time interval between AEWs downstream (to the west) over central and western North Africa. The cyclonic vorticity perturbation started around 8/11/06Z near southwest Arabian Peninsula eventually evolved into the pre-Debby AEW downstream of northern EH ($\sim 38^\circ\text{--}40^\circ\text{E}$). Unlike the pre-Debby MCS which can only be identified clearly from satellite imagery starting at 8/16/18Z, the pre-Debby AEW can be traced almost continuously back to 8/11/06Z.

In summary, the pre-Debby (2006) MCS can be clearly traced back to 8/16/18Z while the convective cloud clusters preceding the MCS can be traced to southwest Arabian Peninsula. The AEW/vorticity perturbations can be traced more continuously to the southwest Arabian Peninsula.

Thus, we may conclude that the pre-Debby (2006) MCS–AEW system was originated from the southwest Arabian Peninsula in the vicinity of the ITCZ. The sources of the convective cloud clusters and vorticity perturbations were attributed to the cyclonic convergence of northeasterly Shamal wind and the Somali jet, especially when the Mediterranean High shifted toward east with high pressure ridge extended farther to the southeast and the Indian Ocean high strengthened and its associated Somali jet penetrated farther to the north. The cyclonic vorticity perturbations were strengthened by the vorticity stretching associated with convective cloud clusters and the convective cloud clusters are strengthened by the diurnal convection over the Sarawat Mountains, Asir Mountains, Ethiopian Highlands, and Darfur Mountains downstream of the genesis region—southwest Arabian Peninsula. The situation may be summarized in the conceptual model shown in Fig. 17.

In general, the ARW simulated pre-Debby AEW/vorticity perturbations and MCS/convective cloud clusters were in good agreement with satellite imagery and global (GFS) model results. However, some discrepancies still existed in their intensity, timing of occurrence and dissipation, and propagation speed. This might be contributed by several factors, such as the relatively coarse resolution of the model, initialization from the global analysis data (GFS), and sensitivity to parameterization schemes, including microphysics, planetary boundary layer, and cumulus parameterizations. Thus, more sensitivity tests are needed to make an optimal combination of parameterizations.

In this study, we have focused on tracing the origins of the pre-Debby MCS/convective cloud clusters and pre-Debby AEW/vorticity perturbations without paying enough attention to the formation of generation mechanisms of these systems. A further study is required to understand exact mechanisms. Such a study might involve a more thorough analysis of global data, and perform a systematic sensitivity tests on isolating forcing mechanisms, such as deactivate sensible and/or latent heating, and removing mountains. To generalize the finding of the origins and the formation mechanism(s) of a pre-TC MCS/cloud clusters and AEW/vorticity perturbations, we have to investigate more cases by performing climatological studies and synoptic in the vicinity of their genesis region. In addition, there are several important problems that remain to be resolved, such as the influence of the diurnal cycle and orographic forcing on MCSs and AEWs, the maintenance and evolution of the pre-Debby MCS and AEW as they propagate across the African continent, and why the previous and next MCSs and AEWs did not evolve into tropical storms, and makes those considered here special. The MCSs and AEWs which did not evolve into tropical cyclones must have been influenced by other

necessary factors for TC genesis, such as low SST, strong vertical wind shear, lack of upper-level trough, thick Saharan air layer, etc. (e.g., see Gray 1998 or Lin 2007 for a brief review). However, the formation of TC, although important, is not the focus of this study. This problem deserves a separate study.

Acknowledgments We would like to thank Dr. Solomon Bililign, the Director of NOAA ISET Center, for his continuous encouragement in pursuing this study. This research was supported by the National Oceanic and Atmospheric Administration Educational Partnership Program under Cooperative Agreement No: NA06OAR4 810187. Reviewers' comments are appreciated, which have improved the quality of the paper significantly.

Appendix: the numerical model and experiment design

The model used for this study is the ARW model version 3.1 (Skamarock 2008). ARW model is a fully compressible, three-dimensional, non-hydrostatic model using terrain-following vertical coordinates. The governing equations for ARW are written in flux-form with conserved mass and dry entropy. In this study, the Runge–Kutta third-order time scheme is employed, and the fifth- and third-order advection schemes are used for the horizontal and vertical directions, respectively.

For the experiments, we utilize a double-nested, two-way interaction domain as illustrated in Fig. 2. For the outer domain, 24 km horizontal resolution with 384×174 horizontal grid intervals is used. In the vertical direction, the grids are stretched from the surface to the model top (20 km) with a total of 28 levels. A 5 km deep sponge layer was added to the upper part of the physical domain. A nudging–relaxation lateral boundary condition is applied at the boundaries of the outer domain. The boundary values are specified by the National Centers for Environmental Prediction (NCEP) GFS reanalysis data, while the relaxation zone includes 4 grid points inward from the lateral boundary. For the inner (nested) domain, a horizontal grid resolution of 8 km is used, which includes 679×283 grid intervals. The vertical grids are stretched as that in the outer domain. The outer (24 km grid spacing) domain is integrated from 8/10/00Z to 8/24/00Z 2006 and initialized by the NCEP GFS reanalysis data, while the inner domain is integrated from 8/11/12Z to 8/18/00Z for the control case (CNTL). These two nested domains are designed to capture the entire lifecycle over Africa for the larger domain and to focus on the development of the pre-Debby MCS/cloud clusters and AEW and their merging for the inner domain.

The following model physics parameterization or representation schemes are chosen for the present simulations:

- Kain–Fritsch cumulus parameterization scheme;
- Thompson microphysics parameterization scheme;
- YSU PBL parameterization scheme;
- Monin–Obukov surface layer scheme;
- Unified NOAA land-surface processes scheme;
- Second-order diffusion term on coordinate surfaces for turbulence and mixing processes;
- Horizontal Smagorinsky first-order closure for eddy coefficient option;
- RRTM longwave radiation parameterization scheme;
- Dudhia shortwave radiation parameterization scheme.

Details of the above schemes and their relevant references can be found in the ARW user manual (Skamarock 2008).

In making the ARW simulations, we found that the numerically simulated results are sensitive to the microphysics parameterization schemes. In order to choose a better scheme, we performed three testing cases with the Thompson, Purdue–Lin, and WSM6 microphysics parameterization schemes (MPSs) which produce slightly different results (not shown). In general, the simulated OLR, relative vorticity and flow fields compared reasonably well with corresponding observed fields except the propagation speeds of the simulated MCCs and MCSs. The Thompson MPS simulates a propagation speed 7.6 ms^{-1} which compares more favorably with the observed propagation speed of 7.4 ms^{-1} than the 6.4 ms^{-1} simulated by the Purdue–Lin and WSM6 MPSs. Thus, we choose the case with Thompson MPS as the control case (Case CNTL) and the Thompson MPS will be used for the numerical experiments in the rest of the paper.

References

- AMMA (2006) African Monsoon Multidisciplinary Analysis: <http://www.amma-international.org/>
- Berry GJ, Thorncroft C (2005) Case study of an intense African easterly wave. *Mon Weather Rev* 133:752–766
- Bister M, Emanuel KA (1997) The genesis of Hurricane Guillermo: TEXMEX analysis and a modeling study. *Mon Weather Rev* 125:2662–2682
- Burpee RW (1972) The origin and structure of easterly waves in the lower troposphere of North Africa. *J Atmos Sci* 29:77–90
- Burpee RW (1974) Characteristics of the North African easterly waves during the summers of 1968 and 1969. *J Atmos Sci* 31:1556–1570
- Carlson TN (1969) Synoptic histories of three African disturbances that developed into Atlantic hurricanes. *Mon Weather Rev* 97:256–276
- Chang CB (1993) Impact of desert environment on the genesis of African wave disturbances. *J Atmos Sci* 50:2137–2145
- Charney JG, Stern ME (1962) On the stability of internal baroclinic jets in a rotating atmosphere. *J Atmos Sci* 19:159–172
- Chen T-C (2006) Characteristics of African easterly waves depicted by ECMWF reanalysis for 1991–2000. *Mon Weather Rev* 134:3539–3566
- Chen S-H, Sun W-Y (2002) A one-dimensional time-dependent cloud model. *J Meteorol Soc Japan* 80:99–118

- Cotton WR, George RL, Wetzel PJ, McAnelly RL (1983) A long-lived mesoscale convective complex. Part I: the mountain-generated component. *Mon Weather Rev* 111:1893–1918
- Farfan LM, Zehnder JA (1997) Orographic influence in the synoptic-scale circulation associated with the genesis of Hurricane Guillermo. *Mon Weather Rev* 125:2683–2698
- Fink AH, Reiner A (2003) Spatio-temporal variability of the relation between African easterly waves and West African squall lines in 1998 and 1999. *J Geophys Res* 108:4332. doi:[10.1029/2002JD002816](https://doi.org/10.1029/2002JD002816)
- Frank NL (1970) Atlantic tropical systems of 1969. *Mon Weather Rev* 98:307–314
- Glickman TS (2000) (ed) *Glossary of meteorology*, 2nd edn. American Meteorological Society
- Goldenberg SB, Shapiro LJ (1996) Physical mechanisms for the association of El Niño and West African rainfall with Atlantic major hurricane activity. *J Clim* 9:1169–1187
- Gray WM (1998) The formation of tropical cyclones. *Meteorol Atmos Phys* 67:37–69
- Grist JP, Nicholson SE, Barcilon AL (2002) Easterly wave over Africa. Part II: observed and modeled contrast between wet and dry years. *Mon Weather Rev* 130:212–225
- Hill CM, Lin Y-L (2003) Initiation of a mesoscale convective complex over the Ethiopian Highlands preceding the genesis of Hurricane Alberto (2000). *Geophys Res Lett* 30(5):1232. doi:[10.1029/2002GL016655](https://doi.org/10.1029/2002GL016655),2003
- Holton JR (2004) *An introduction to dynamic meteorology*, 4th edn. Elsevier Academic Press, Amsterdam
- Houze RA (1993) *Cloud dynamics*. Academic Press, New York
- Hsieh J-S, Cook KH (2005) Generation of African easterly wave disturbances: relationship to the African easterly jet. *Mon Weather Rev* 133:1311–1327
- Hsieh J-S, Cook KH (2007) A study of the energetics of African easterly waves using a regional climate model. *J Atmos Sci* 64:2212–2230
- Kwon HJ (1989) A re-examination of the genesis of African waves. *J Atmos Sci* 46:3621–3631
- Laing AG, Fritsch JM (1993) Mesoscale convective complexes in Africa. *Mon Weather Rev* 121:2254–2263
- Laing A, Carbone R, Levizzani V, Tuttle J (2008) The propagation and diurnal cycles of deep convection in northern tropical Africa. *Q J R Meteorol Soc* 134:93–109
- Landsea CW (1993) A climatology of intense (or major) Atlantic hurricanes. *Mon Weather Rev* 121:1703–1713
- Lin Y-L (2007) *Mesoscale dynamics*. Cambridge University Press, Cambridge
- Lin Y-L, Robertson KE, Hill CM (2005) Origin and propagation of a disturbance associated with an African easterly wave as a precursor of Hurricane Alberto (2000). *Mon Weather Rev* 133:3276–3298
- Mass C (1979) A linear primitive equation model of African wave disturbances. *J Atmos Sci* 36:2075–2092
- Mekonnen A, Thorncroft CD, Aiyyer AR (2006) Analysis of convection and its association with African easterly waves. *J Climate* 19:5405–5421
- Mozer JB, Zehnder JA (1995) Lee vorticity production by large-scale tropical mountain ranges. Part II: a mechanism for the production of African waves. *J Atmos Sci* 53:539–549
- NOAA (2006) NOAA CPC FEWS—NET Rainfall Estimate (mm): for the Northern Africa Rainfall Climatology, August 2006. (<http://www.cpc.ncep.noaa.gov/products/fews/rfe1.shtml>)
- Payne SW, McGarry MM (1977) The relationship of satellite inferred convective activity to easterly waves over West Africa and the adjacent ocean during phase III of GATE. *Mon Weather Rev* 105:413–420
- Pielke RA Jr, Landsea CW (1998) Normalized hurricane damages in the United States: 1925–1995. *Weather Forecast* 13:621–631
- Pytharoulis I, Thorncroft C (1999) The low-level structure of African easterly waves in 1995. *Mon Weather Rev* 127:2266–2280
- Rao PG, Hatwar HR, Al-Sulaiti HH, Al-Mulia AH (2003) Summer shamals over the Arabian Gulf. *Weather* 58:472–478
- Reed RJ, Norquist DC, Recker EE (1977) The structure and properties of African wave disturbances as observed during phase III of GATE. *Mon Weather Rev* 105:317–333
- Rennick MA (1976) The generation of African waves. *J Atmos Sci* 33:1955–1969
- Seo H, Jochum M, Murtugudde R, Miller AJ, Roads JO (2008) Precipitation from African easterly waves in a coupled model of the tropical Atlantic. *J Climate* 21:1417–1431
- Simmons AJ (1977) A note on the instability of the African easterly jet. *J Atmos Sci* 34:1670–1674
- Skamarock WC, Klemp JB, Dudhia J, Gill DO, Barker DM, Duda MG, Huang X-Y, Wang W, Powers JG (2008) A description of the advanced research WRF version 3. NCAR technical note. (http://www.mmm.ucar.edu/wrf/users/docs/arw_v3.pdf)
- Thorncroft CD (1995) An idealized study of African easterly waves. Part III: more realistic basic states. *Q J R Meteorol Soc* 121:1589–1614
- Thorncroft CD, Hoskins BJ (1994a) An idealized study of African easterly waves. Part I: a linear view. *Q J R Meteorol Soc* 120:953–982
- Thorncroft CD, Hoskins BJ (1994b) An idealized study of African easterly waves. Part II: a nonlinear view. *Q J R Meteorol Soc* 120:983–1015
- Thorncroft CD, Hall NM, Kiladis GN (2008) Three-dimensional structure and dynamics of African easterly waves. Part III: genesis. *J Atmos Sci* 65:3596–3607
- Wetzel PJ, Cotton WR, McAnelly RL (1983) A long-lived mesoscale convective complex. Part II: evolution and structure of the mature complex. *Mon Weather Rev* 111:1919–1937